PHYSICAL REVIEW D **82,** 035010 (2010)

μ to e in R-symmetric supersymmetry

Ricky Fok and Graham D. Kribs

Department of Physics, University of Oregon, Eugene, Oregon, 97403, USA

(Received 14 April 2010; published 16 August 2010)

We demonstrate that $\mu \leftrightarrow e$ slepton mixing is significantly more restricted than previously thought within the already remarkably flavor-safe R-symmetric supersymmetric standard model. We calculate bounds from $\mu \to e\gamma$, $\mu \to 3e$, and most importantly, $\mu \to e$ conversion. The process of $\mu \to e$ conversion is significantly more restrictive in R-symmetric models since this process can occur through operators that do not require a chirality flip. We delineate the allowed parameter space, demonstrating that maximal mixing is rarely possible with weak scale superpartners, while $\mathcal{O}(0.1)$ mixing is permitted within most of the space. The best approach to find or rule out $\mu \leftrightarrow e$ mixing in R-symmetric supersymmetric models is a multipronged attack looking at both $\mu \to e$ conversion as well as $\mu \to e\gamma$. The redundancy eliminates much of the parameter space where one process, but not both processes, contains amplitudes that accidentally destructively interfere. We briefly discuss implications for searches of slepton flavor violation at the LHC.

DOI: 10.1103/PhysRevD.82.035010 PACS numbers: 12.60.Jv, 13.35.−r, 14.80.Ly

I. INTRODUCTION

Lepton flavor violation (LFV) is predicted to occur at an unobservably small rate in the standard model. In low energy supersymmetric theories, new sources of lepton flavor violation are generic in the soft breaking sector. The experimental nonobservation of $\mu \to e$ processes is particularly restrictive, given the impressive bounds on $\mu \to e\gamma$ from MEGA [1] and MEG [2], on $\mu \to e$ conversion from SINDRUM II [3], and to a lesser extent from $\mu \to 3e$ from SINDRUM [4]. Further progress is expected from the varied experiments that are ongoing as well as planned future experiments such as Mu2e [5] and other proposals utilizing Project X at Fermilab [6].

In the minimal supersymmetric standard model (MSSM), $\mu \leftrightarrow e$ mixing is severely constrained by these bounds (e.g., [7–11]). The size of the mixing can be characterized by the quantity $\delta^{\ell}_{XY} \equiv \delta m^2_{XY}/m^2$, where δm^2_{XY} is the off-diagonal (12) entry appearing in the sfermion mass matrix connecting the X-handed slepton to the Y-handed slepton, and m^2 is the average slepton mass. Reference [11] found $\delta^{\ell}_{LR} \lesssim 3 \times 10^{-5}$, while $\delta^{\ell}_{LL} \lesssim 6 \times 10^{-4}$ over a scan of the minimal supergravity parameter space. Similarly strong bounds on δ^{ℓ}_{RR} can also be found, though cancellations between diagrams in the amplitude can in some cases allow for much larger mixing [9–11].

Recently, a new approach to weak scale supersymmetry that incorporates an extended R-symmetry [12] suggests large flavor violation in the supersymmetry breaking parameters may be present *without* exceeding the flavor-violating bounds. This is possible for several reasons: R-symmetric supersymmetry has no flavor-violating LR mixing, solving the worst of the problem trivially. R-symmetric supersymmetry has Dirac gauginos and no Majorana masses, removing all dimension-5 flavor-violating operators. Finally, R-symmetric supersymmetry also has no flavor-conserving LR mixing, and so there are no "large tanβ enhanced" effects. These benefits were found to virtually eliminate constraints on the slepton flavor mixing [12].

In this paper, we reconsider the constraints on slepton mixing, specifically, $\mu \leftrightarrow e$ mixing. Unlike the MSSM, the most important constraint is not necessarily $\mu \to e\gamma$. This is easily seen by inspection of the R-symmetric flavor-violating operators: $\mu \to e\gamma$ requires a chirality flip via a muon Yukawa coupling; whereas, $\mu \to e$ conversion has no such requirement. We find that $\mu \to e$ conversion rules out maximal mixing throughout the right-handed slepton mixing parameter space for sub-TeV superpartner masses. This is complementary to $\mu \to e\gamma$, where we find cancellations between the bino and Higgsino diagrams, analogous to what was found before in the MSSM [9–11]. For left-handed slepton mixing, we find possible cancellations in the amplitudes for $\mu \to e$ conversion, and instead $\mu \to e\gamma$ provides generally the strongest constraint. We also calculated $\mu \to 3e$ and find it provides the weakest constraint on both left-handed and right-handed slepton mixing throughout the parameter space we consider.

This paper is organized in as follows: We review the relevant characteristics of a model with an extended R-symmetry, and the super–Glashow-Iliopoulos-Maiani (GIM) mechanism in Sec. II. In Sec. III, we begin the discussion of experimental constrains on the parameters from $\mu \to e\gamma$ in Sec. III A, $\mu \to e$ conversion in Sec. III B, and finally, $\mu \to 3e$ in Sec. III C. In Sec. IV, we briefly discuss implications for slepton flavor violation to be observed at LHC. Finally, in Sec. V, we conclude with a discussion of our results.

II. A SIMPLIFIED R-SYMMETRIC MODEL

We are interested in analyzing LFV in the minimal R-symmetric standard model (MRSSM). The gaugino structure of the MRSSM has been studied in detail in

Ref. [13], where the mixings and couplings of the four Dirac neutralinos and four Dirac charginos are given. Weak scale supersymmetry with Dirac gauginos is a possibility that was contemplated some time ago in [14–16] and more recently in [12,13,17–32]. A fully general analysis of LFV in the MRSSM would be a substantial undertaking. Fortunately, there are several simplifications we can employ to gain a fairly general understanding of the allowed parameter space of LFV in the MRSSM. One important restriction is that the Dirac wino cannot be light in the MRSSM, due to the structure of the wino supersoft operator [17]. Essentially, there is an unavoidable contribution to the vacuum expectation value of the $SU(2)_L$-triplet scalar that causes a contribution to the ρ parameter that is too large unless the wino is above about a TeV. Second, since there is no coupling between up-type Higgs and leptons, the contribution from the up-type Higgsino eigenstates is suppressed by the small mixing between bino or $\tilde{H}_d$ and $\tilde{H}_u$, and so it can be ignored.

Itemizing the simplifications, we take the following.

(1) The wino mass, M_2, is taken to be sufficiently large so as to give negligible contribution to flavor-violating interactions. This simplification means that the ρ parameter is automatically safe throughout the parameter space we consider.

(2) The up-type Higgsino mass μ_u, is also taken to be large for convenience. Since the up-type Higgsinos play no role whatsoever in charged lepton flavor violation (given also point 1), this is done simply to keep the gaugino sector to a 2×2 structure and thus easily understood. (We will, however, consider effects of a light up-type Higgsino on flavor-violating signals at LHC in Sec. IV.)

(3) We consider left-handed and right-handed slepton mixing separately. This is standard practice when considering flavor violation in the MSSM (e.g., [11]). We will see that there are qualitative differences between the allowed parameter space of left-handed and right-handed slepton mixing.

(4) We assume the slepton mixing is purely in the 2×2 flavor space of e, μ. Enlarging this mixing to the full 3×3 mixing does not qualitatively change any of our results, and instead simply dilutes the effect of the mixing, while adding more mixing angles and thus more parameters to the model. Since the focus of this paper is to explore $\mu \leftrightarrow e$ mixing, no further discussion of the 3×3 case will be given.

(5) For our numerical results, we take $m_{\tilde{l}_2} = 1.5 m_{\tilde{l}_1}$. This seems a far more drastic assumption than it actually is. Our motivation is to consider slepton flavor violation when there is essentially *no degeneracy* among the sleptons, and so we took the slepton mass ratio to be "order one" but not near one. Taking the ratio much larger than 1 does not appreciably increase the flavor violation, while taking it smaller causes the super-GIM mechanism to suppress the flavor-violating signal. Our compromise is the above number.

In Appendix, we provide more details on the gaugino structure and flavor-violating interactions as directly relevant to this paper. With the above assumptions, there is only one light Dirac chargino (which is $\tilde{H}_d^{\pm}$-like) and two light Dirac neutralinos (which are mixtures of $\tilde{H}_d^0$ and $\tilde{B}$).

A few more comments on the slepton mass eigenstate hierarchy are in order. MSSM analyses of slepton flavor violation have, by necessity of LFV constraints, concentrated on the case where the mass difference between the different states is small, $\Delta^2 \equiv m_{\tilde{l}_2}^2 - m_{\tilde{l}_1}^2 \ll m_{\tilde{l}_{1,2}}^2$. In this limit, it is straightforward to show that the contribution to LFV can be expanded in powers of Δ^2, taking the form

$$\sin 2\theta_l \left(\frac{\Delta^2}{M_{\mathrm{SUSY}}^2} + \cdots \right), \tag{2.1}$$

where M_{SUSY} is typically the largest mass sparticle in the diagram that dominates the process. There is no Δ-independent contribution within the parentheses due to the super-GIM mechanism (see the next section). Since $\sin 2\theta_l = 2m_{e\mu}^2/\Delta^2$, one factor of Δ^2 cancels, giving proportionality to the δ parameter mentioned in the introduction and used in many other papers on LFV in the MSSM (at least up to a possible further suppression of $|m_{\tilde{l}_1} m_{\tilde{l}_2}|/m_{N,C}^2$ if $m_{N,C} \gg m_{\tilde{l}_{1,2}}$).

In this paper, Δ^2 is not small, and so using the "δ parameter" is simply not appropriate. Instead, it is easy to see that in the opposite limit, $\Delta^2 \gg m_{\tilde{l}_1}^2$, the contributions to LFV are proportional to simply $\sin 2\theta_l / m_{\tilde{l}_1}^2$. Hence, the relevant parameters we show in most of our numerical results are bounds on $\sin 2\theta_l$ as a function of the slepton, gaugino, and Higgsino masses. Reducing the splitting can be roughly approximated by relaxing the constraint on $\sin 2\theta_l$ by ratios of $\Delta_{\mathrm{old}}^2/\Delta_{\mathrm{new}}^2$.

The super-GIM mechanism

The "super-GIM mechanism"—the GIM mechanism applied to flavor in the superpartner sector—is important in understanding the phenomena of flavor violation. As it is well known, the super-GIM mechanism arises as a consequence of the unitarity of the slepton mixing matrices that diagonalize the mass matrix; $U_{ik}^{\dagger} U_{kj} = \delta_{ij}$, where the sum over repeated indices is performed. This combination of mixing matrix elements always appears as a prefactor in the calculation of amplitudes of flavor-violating processes. Specifically for our case of slepton flavor violation, we have $U_{ek}^{\dagger} U_{k\mu} = 0$, corresponding to an incoming muon, and an outgoing electron, with internal sleptons labeled by k. The sum over k corresponds to summing over all mass eigenstate sleptons $\tilde{l}_k$ in the loop. There are two immediate consequences of the super-GIM mechanism.

First, terms that do not depend on the slepton masses do not contribute. Let $f(m_k)$ be some function that depends on the mass of the sleptons and α be some quantity that does not depend on m_k, then

$$\sum_k U^\dagger_{ek} U_{k\mu}[\alpha + f(m_k)] = \sum_k U^\dagger_{ek} U_{k\mu} f(m_k). \quad (2.2)$$

The form of Eq. (2.2) appears when a logarithmic divergent loop integral is dimensionally regularized, and one finds the $1/\epsilon$ term appearing as a constant term α in the above equation. This leads to an important result: the would-be logarithmic UV divergence in flavor-conserving processes is, in fact, UV finite in flavor-violating processes. In this paper, unless otherwise stated, we will omit the terms in our expressions that are canceled by the super-GIM mechanism.

The other well-known consequence is that, when all the sleptons are degenerate, there is no flavor violation. This can be seen again in Eq. (2.2) with $m_k = m$, the sum over all slepton flavors in a flavor-violating process vanishes.

III. EXPERIMENTAL CONSTRAINTS

There are three $\mu \to e$ conversion processes with experimental bounds: $\mu \to e\gamma$, $\mu \to e$ conversion, and $\mu \to 3e$. In this section we present our calculations of the rates of these processes and present results in terms of a series of contour plots showing the allowed parameter space.

The rate for $\mu \to e\gamma$ was estimated in Ref. [12] in the slepton flavor-violating mass-insertion approximation with a pure bino and wino and a specific gaugino hierarchy. In this paper we have neglected the wino, due to the ρ parameter constraint, and instead included the down-type Higgsino $\tilde{H}^0_d$. Since we have considered large mixing angles, up to and including maximal mixing, we have diagonalized the slepton masses explicitly and done our loop calculations involving the slepton mass eigenstates.

As stated in our simplifications, we have not included contributions from the wino or up-type Higgsino. We focus on the case where the sleptons and the lighter neutralinos are in the sub-TeV range where wino contributions can be reasonably ignored. The up-type Higgsino does not couple to leptons, and we take the light quark Yukawa couplings to vanish. Thus, the up-type Higgsino does not give a significant contribution to any of $\mu \to e\gamma$, $\mu \to e$ conversion in nuclei and $\mu \to 3e$.

With these simplifications, the amplitudes of LFV processes are sensitive to just two neutralinos, mixtures of $\tilde{B}$ and $\tilde{H}^0_d$ inside the loops. We can also neglect the contributions due to charginos, because the only light chargino is $\tilde{H}^0_d$-like. Hence, all types of diagrams we consider involving a chargino are suppressed not only by one power of muon Yukawa, but also one power of either the electron Yukawa, or the tiny wino content of the light chargino at the lepton-chargino-sneutrino vertex. This also means that sneutrino mixing does not contribute to LFV processes, and thus the difference in the amplitudes between left-handed and right-handed slepton mixing is due solely to the hypercharges and masses of the left-handed and right-handed charged leptons.

A. $\mu \to e\gamma$

The neutrinoless muon decay $\mu \to e\gamma$ occurs through the effective magnetic dipole moment operator, $\bar{e}\sigma_{\mu\nu}F^{\mu\nu}\mu$, and requires a chirality flip of fermions. There are no tree level operators that lead to this decay, and the lowest order is at one loop. In the MRSSM, there are only two types of contributions to the $\mu \to e\gamma$ amplitude: one where the chirality flip occurs on the external muon line, and the other where the flip occurs as a result of a muon-smuon-Higgsino vertex proportional to the muon Yukawa coupling. The diagrams are shown in Fig. 1.

We calculated the amplitudes in the mass eigenstate basis of the sleptons and neutralinos, and as a check we derived the results obtained in Ref. [8] (replacing their $\tilde{\mu}$-$\tilde{\tau}$ mixing with $\tilde{e}$-$\tilde{\mu}$ mixing). The effective Lagrangian is

$$\mathcal{L}_{\text{eff}} = \frac{m_\mu}{2}\bar{e}\sigma_{\mu\nu}F^{\mu\nu}(A^L_{\gamma\text{dip}}P_L + A^R_{\gamma\text{dip}}P_R)\mu. \quad (3.1)$$

We rewrite the amplitudes $A^L_{\gamma\text{dip}}$ and $A^R_{\gamma\text{dip}}$, as

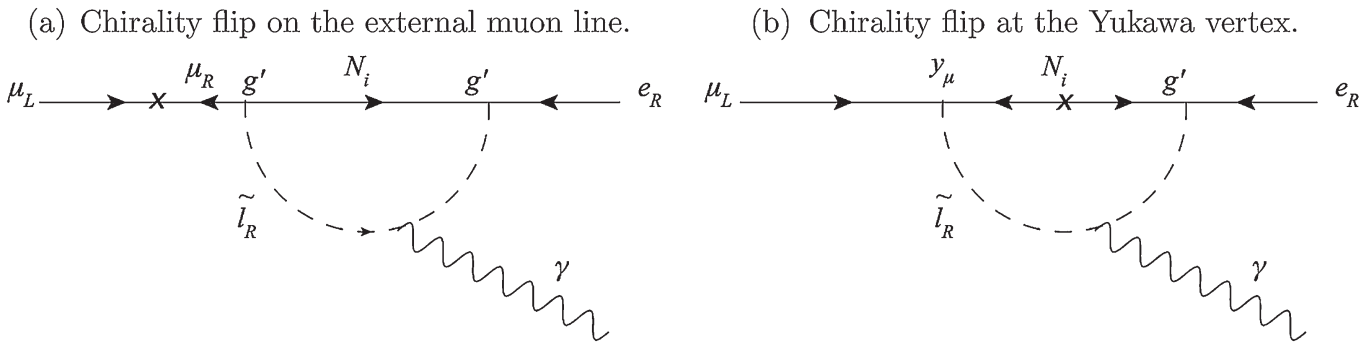

FIG. 1. Feynman diagrams for $\mu \to e\gamma$ corresponding to the amplitudes (a) A_{Rin1} and (b) A_{Rin2} mediated by right-handed slepton flavor mixing. The diagrams for left-handed slepton flavor mixing are obtained by swapping $L \leftrightarrow R$.

$$A^L_{\gamma\mathrm{dip}} = \sum_{i=1}^{2}(A_{Lin1} + A_{Lin2}), \tag{3.2}$$

$$A^R_{\gamma\mathrm{dip}} = \sum_{i=1}^{2}(A_{Rin1} + A_{Rin2}), \tag{3.3}$$

where the sum is over the ith neutralinos. The subscripts 1 and 2 denote the locations of the chirality flip on the muon line and at the muon-slepton-gaugino vertex, respectively. As we shall see below, for right-handed sleptons there can be an accidental cancellation between amplitudes involving these diagrams.

The $\mu \to e\gamma$ branching ratio is given by

$$\mathrm{BR}(\mu \to e\gamma) = \frac{48\alpha\pi^3 m_\mu^2}{G_F^2}[|A^L_{\gamma\mathrm{dip}}|^2 + |A^R_{\gamma\mathrm{dip}}|^2], \tag{3.4}$$

with the amplitudes involving a neutralino N_i and sleptons $\tilde{l}_1$ and $\tilde{l}_2$ with the sleptons mass-ordered as $m_{\tilde{l}_1} < m_{\tilde{l}_2}$. The amplitudes involving right-handed sleptons are

$$A_{Rin1} = \frac{(Y^l_R)^2 g'^2}{3(16\pi^2)}(O_{Li\tilde{B}})^2 \cos\theta_{\tilde{l}} \sin\theta_{\tilde{l}}\left[\frac{f_{n1}(x_{1i})}{m^2_{\tilde{l}_{R1}}} - \frac{f_{n1}(x_{2i})}{m^2_{\tilde{l}_{R2}}}\right], \tag{3.5}$$

$$A_{Rin2} = \frac{Y^l_R g'^2 m_{N_i}}{2(16\pi^2)M_Z \sin\theta_w \cos\beta} O_{Ri\tilde{H}^0_d} O_{Li\tilde{B}} \cos\theta_{\tilde{l}} \sin\theta_{\tilde{l}} \times \left[\frac{f_{n2}(x_{1i})}{m^2_{\tilde{l}_{R1}}} - \frac{f_{n2}(x_{2i})}{m^2_{\tilde{l}_{R2}}}\right], \tag{3.6}$$

where A_{Rin1} is the amplitude that involves an external chirality flip of the muon and A_{Rin2} involves a flip at the Higgsino vertex. Here, $O_{Ri\tilde{H}^0_d}$ and $O_{Li\tilde{B}}$ are the Higgsino and bino content of N_i, respectively, (i.e., the corresponding elements in the orthogonal matrices that diagonalize the gaugino mass matrix squared), and $Y^l_R = Y^{l^c} = +1$. To lowest nonvanishing order in M_Z, the neutralino mixings are (dropping the subscripts L and R from now on)

$$O_{1\tilde{B}}(\mu_d \ll M_1) = O_{1\tilde{H}^0_d}(\mu_d \gg M_1) = \frac{\cos\beta \sin\theta_w M_Z \mu_d}{M_1^2 - \mu_d^2}, \tag{3.7}$$

$$O_{2\tilde{B}}(\mu_d \gg M_1) = O_{2\tilde{H}^0_d}(\mu_d \ll M_1) = -\frac{\cos\beta \sin\theta_w M_Z M_1}{M_1^2 - \mu_d^2}, \tag{3.8}$$

and $O_{i(\tilde{B},\tilde{H}^0_d)} = 1$ in the appropriate limits. The functions $f_{nj}(x_i)$, with $x_{ik} = m^2_{N_k}/m^2_{\tilde{l}_{Ri}}$, with $j = 1, 2$, come from integrating over the loops in the diagrams:

$$f_{n1}(x) = \frac{1}{2(1-x)^4}(1 - 6x + 3x^2 + 2x^3 - 6x^2 \ln x), \tag{3.9}$$

$$f_{n2}(x) = \frac{1}{(1-x)^3}(1 - x^2 + 2x \ln x). \tag{3.10}$$

Finally, the amplitudes for the left-handed sleptons can be obtained from the right-handed slepton results by doing the replacements

$$A^R_{\gamma\mathrm{dip}} \to A^L_{\gamma\mathrm{dip}} \quad \text{upon} \quad (Y^l_R, m^2_{\tilde{l}_{Ri}}) \to (Y^l_L, m^2_{\tilde{l}_{Li}}). \tag{3.11}$$

Inserting the results in Eqs. (3.7) and (3.8) into (3.5) and (3.6), we see that to lowest vanishing order in M_Z, $\mathrm{BR}(\mu \to e\gamma)$ is independent of $\tan\beta$. We can also see explicitly that when the two slepton masses are degenerate, the branching ratio vanishes, as expected from the super-GIM mechanism.

As an aside, it is also straightforward to see what happens to the results when the mass hierarchy between the slepton and the neutralino are inverted. The loop functions satisfy the identities,

$$f_{n1}(x) + f_{n1}\left(\frac{1}{x}\right) = \frac{1}{2}, \tag{3.12}$$

$$x f_{n2}(x) - f_{n2}\left(\frac{1}{x}\right) = 0. \tag{3.13}$$

We are now in a position to discuss the amplitudes in various limits. In the bino-like limit $M_1 \ll \mu_d$, one sees that A_{R1n1} dominates, as A_{Rin2} is of order M_1/μ_d.

When N_1 becomes $\tilde{H}^0_d$-like, there is a cancellation between the amplitudes involving a chirality flip on the external muon line, and the one with the flip occurring at the muon Yukawa vertex. The dominant diagram in the $\tilde{B}$-like case, A_{R1n1}, is now suppressed by μ_d^2/M_1^2, the same suppression factor appears A_{R1n2}. So the dominant amplitudes come from the diagrams involving a $\tilde{B}$-like neutralino exchange. Note that A_{R2n2} has an opposite sign compared to A_{R2n1} and the total amplitude can vanish for some choice of parameters.

In Figs. 2(a)–2(d), we show the allowed regions in MRSSM parameter space with right-handed slepton mixing that satisfy the bound $\mathrm{BR}(\mu \to e\gamma) < 1.2 \times 10^{-11}$ [1,2].

The situation is drastically different in the case of left-handed slepton mixing. The hypercharge of the left-handed leptons ($Y^l_L = -1/2$), has an opposite sign to the right-handed lepton hypercharge, and so the amplitudes interfere constructively, instead of destructively as in the case of right-handed slepton mixing. This leads to a more severe bound on the allowable regions in parameter space for left-handed slepton mixing. This is shown in Figs. 3(a)–3(d).

B. $\mu \to e$ conversion in a nucleus

The conversion of a muon into an electron can give a qualitatively distinct bound on $\mu \leftrightarrow e$ slepton mixing because there are several types of operators beyond those that

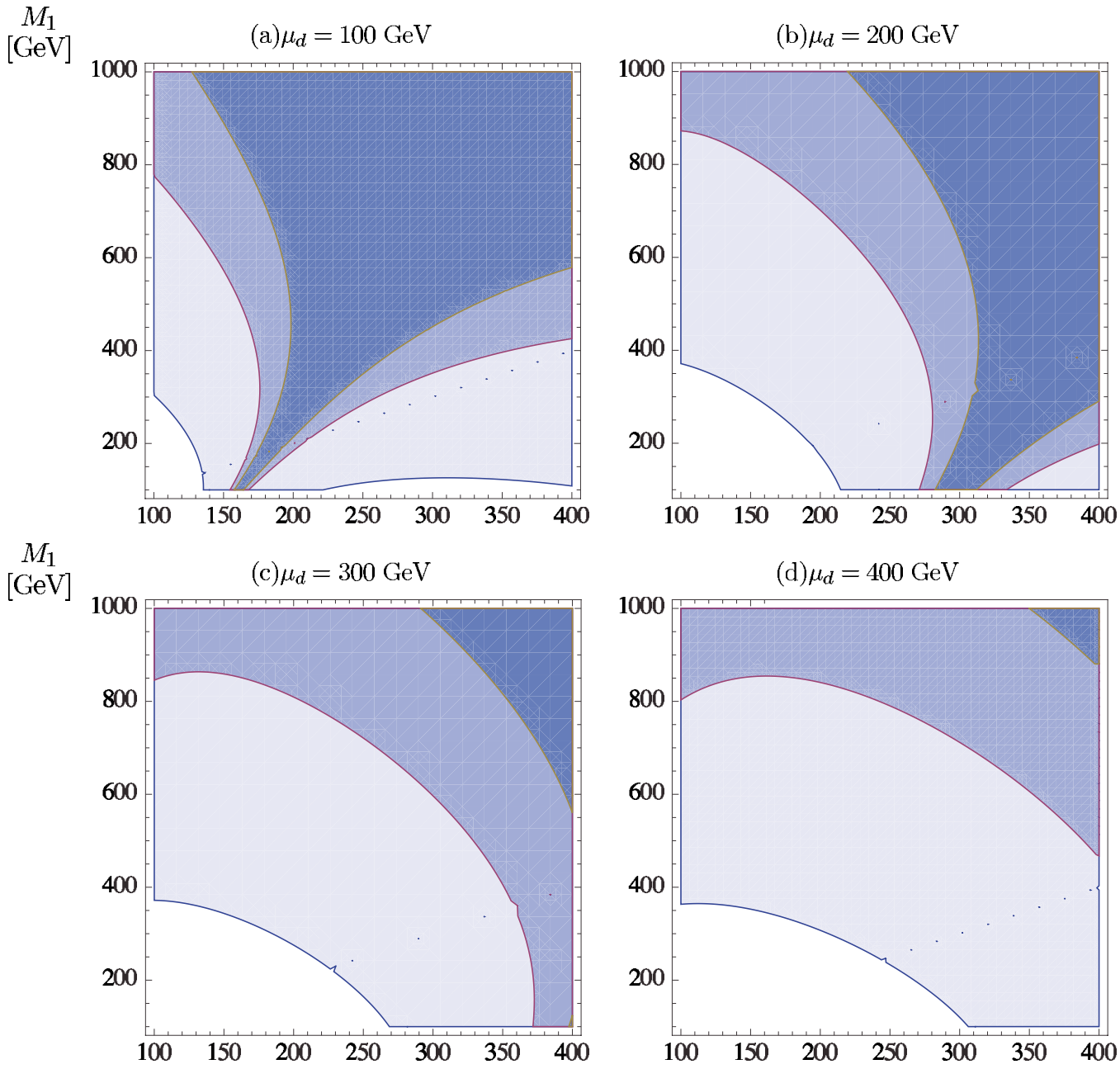

FIG. 2 (color online). Regions in parameter space (shaded) that satisfy the $\mu \to e\gamma$ bound for right-handed slepton mixing. The mass of the heavier slepton is set to $1.5m_{\tilde{l}_1}$. From light to dark, the shaded areas denote mixing with $\sin 2\theta_{\tilde{l}} = 0.1$, 0.5, and 1, respectively. The funnel regions in the plots with $\mu_d = 100$, 200 GeV is caused by the cancellation between the amplitudes involving the bino-like and the $\tilde{H}_d^0$-like neutralinos.

contribute to $\mu \to e\gamma$. We discuss the operators for $\mu \to e$ conversion, one-by-one, in this section.

The $\mu \to e$ conversion amplitude is dominated by coherent processes, and so we only took the quark vector currents into account. The operators that contribute to the incoherent terms, $\bar{q}\gamma^5 q$, $\bar{q}\gamma^\mu\gamma^5 q$, and $\bar{q}\sigma^{\mu\nu} q$ have been neglected. This leaves us with the scalar and vector current, $\bar{q}q$ and $\bar{q}\gamma^\mu q$, respectively [7].

The only diagram that can contribute to a scalar quark current is the box diagram. Without left-right mixing of sleptons in the MRSSM, the dominant term, with bino couplings at each vertex, contains no chirality flip of the quarks, and is therefore a vector current. We also take the quark current to be nonrelativistic to simplify the calculation involving the magnetic dipole term. Thus, the amplitude for $\mu \to e$ conversion is well approximated, for our

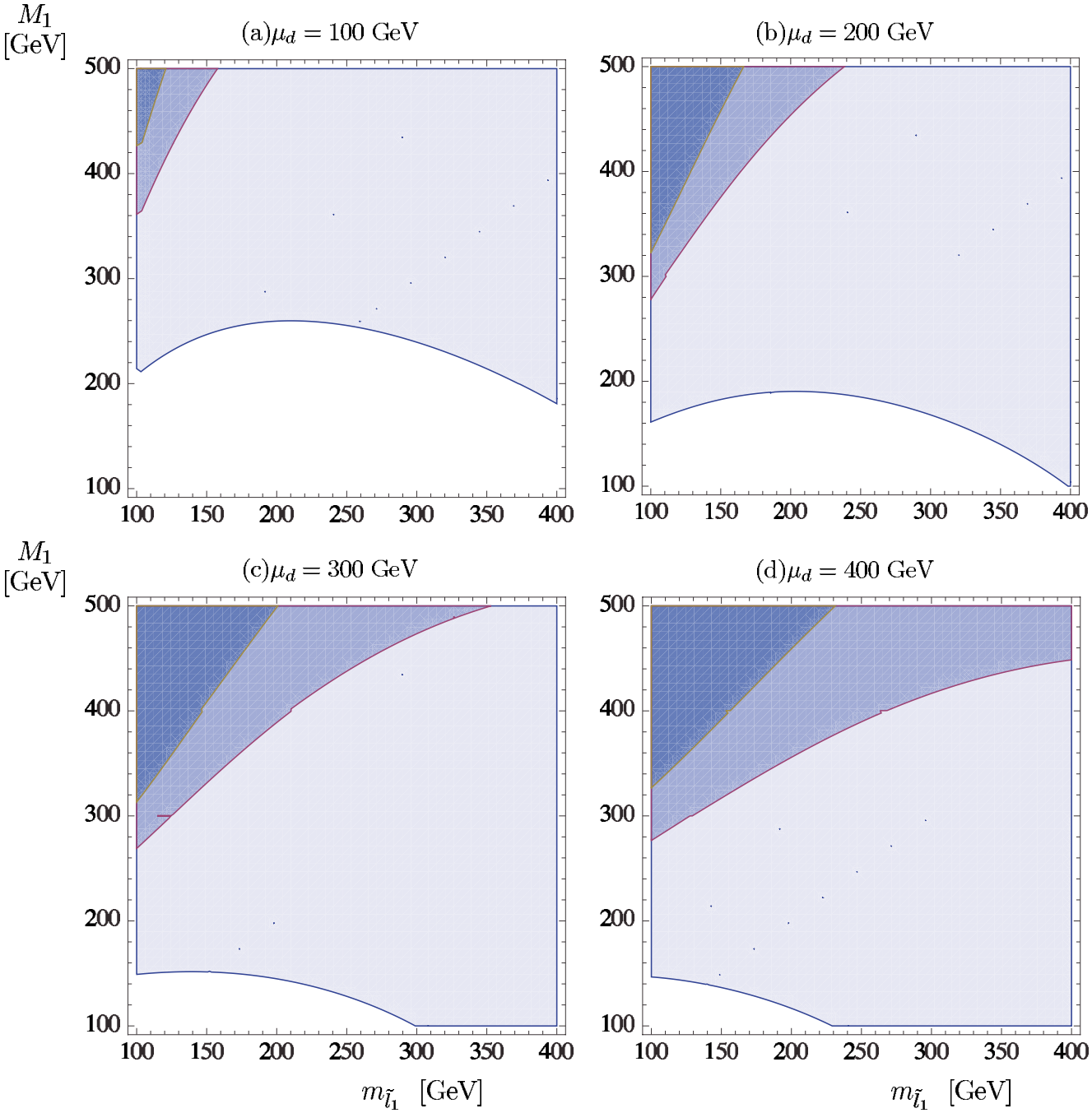

FIG. 3 (color online). Same as Fig. 2 but for left-handed slepton mixing. We have restricted $M_1 < 500$ GeV since contributions from wino-like charginos not been included (see Sec. II for a discussion).

purposes, by only taking quark vector currents into account.

The diagrams we consider are the photon penguin, the Z penguin, and the box diagram shown in Figs. 4–7. We only take the dominant terms of the box and the Z-penguin amplitude into account: that is, the terms involving the bino coupling at each vertex which does not contain any chirality flips of the external fermions. The effective Lagrangian at the parton level can be written as [7]

$$\begin{aligned}\mathcal{L}_{\text{eff}} = \sum_{q=u,d} & -Q_q e^2 \bar{e}\Big[\gamma^\mu (A_\gamma^L P_L + A_\gamma^R P_R) \\ & + \frac{m_\mu}{k^2} i\sigma^{\mu\nu} k_\nu (A_{\gamma\text{dip}}^L P_L + A_{\gamma\text{dip}}^R P_R)\Big]\mu\bar{q}\gamma_\mu q \\ & + e^2 \sum_{q=u,d} \bar{e}\,\gamma^\mu [(A_Z^L + A_{\text{box}}^{qL})P_L \\ & + (A_Z^R + A_{\text{box}}^{qR})P_R]\mu\bar{q}\gamma_\mu q, \end{aligned} \tag{3.14}$$

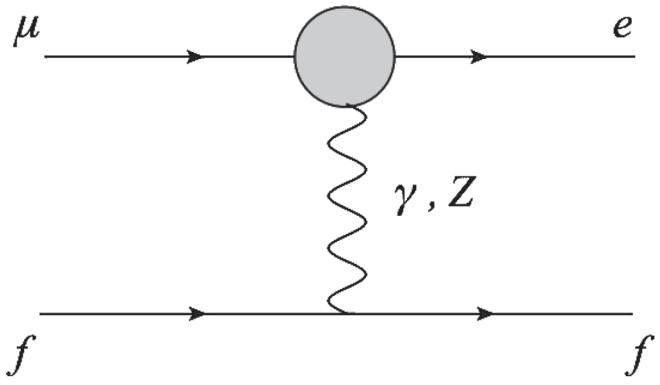

FIG. 4. Schematic diagram illustrating the set of penguin contributions to $\mu \to e$ conversion (for $f = q$) as well as $\mu \to 3e$ (for $f = e$). The blob in the figure arises from both charge radius subdiagrams shown in Fig. 5, as well as Z-penguin subdiagrams, the dominant ones shown in Fig. 6.

where Q_q is the quark electric charge, $k^2 \sim -m_\mu^2$ is the momentum transfer, $A_{\gamma,Z}^{L,R}$ and $A_{\gamma\text{dip},Z}^{L,R}$ correspond to the γ penguin and Z penguin, respectively, and $A_{\text{box}}^{q(L,R)}$ corresponds to the box diagram.

The most severe upper bound to date is on the conversion rate ratio with a gold nucleus. $\text{BR}(\mu \to e)_{\text{Au}} \equiv \Gamma(\mu^- \text{Au} \to e^- \text{Au})/\Gamma(\mu^- \text{Au})_{\text{capture}} < 7 \times 10^{-13}$ from SINDRUM II [3]. Because of the large number of protons in the gold nucleus, the distortion to the muon wave function from a plane wave must be taken into account when evaluating the overlap between the muon and nucleus wavefunctions. This has been done in Ref. [33], and we will use their overlap integrals, with the neutron density determined from pionic atom experiments (method 2 in [33]). Other nuclei could also be of interest, particularly as a way to distinguish different models [34]. The conversion rate is

$$\Gamma_{\mu\to e} = 4m_\mu^5 e^4 |\mathcal{A}_{\gamma\text{dip}}^L + \mathcal{A}_\gamma^R + \mathcal{A}_{\text{box}}^R + \mathcal{A}_Z^R|^2 + (L \leftrightarrow R), \tag{3.15}$$

where

$$\mathcal{A}_{\gamma\text{dip}}^L = -\frac{1}{8e} A_{\gamma\text{dip}}^L D, \tag{3.16}$$

$$\mathcal{A}_\gamma^R = A_\gamma^R V^{(p)}, \tag{3.17}$$

$$\mathcal{A}_{\text{box}}^R = -(2A_{\text{box}}^{uR} + A_{\text{box}}^{dR})V^{(p)} - (A_{\text{box}}^{uR} + 2A_{\text{box}}^{dR})V^{(n)}, \tag{3.18}$$

$$\mathcal{A}_Z^R = [(2Z_u + Z_d)V^{(p)} + (2Z_d + Z_u)V^{(n)}]A_Z^R, \tag{3.19}$$

where $Z_q = (Z_{q_R} + Z_{q_L})/2$, with $Z_{q_{(L,R)}} = I_{L,R}^q - Q\sin^2\theta_w$, $I_L^u = 1/2$, $I_L^d = -1/2$ for up and down-type quarks, and $I_R^q = 0$. The first term in Eq. (3.15), proportional to $|\mathcal{A}_{\gamma\text{dip}}^L + \mathcal{A}_\gamma^R + \mathcal{A}_{\text{box}}^R + \mathcal{A}_Z^R|^2$, corresponds to slepton mixing in the right-handed sector, while the second term proportional to $|\mathcal{A}_{\gamma\text{dip}}^R + \mathcal{A}_\gamma^L + \mathcal{A}_{\text{box}}^L + \mathcal{A}_Z^L|^2$, corresponds to to slepton mixing in the left-handed sector. The coefficients D and $V^{(p,n)}$ are to the overlap integrals of the muon and the nucleus for the leptonic dipole and vector (proton, neutron) operators. We used, for a gold nucleus, $D = 0.167$, $V^{(p)} = 0.0859$, $V^{(n)} = 0.108$ from Ref. [33].

Now we will discuss each diagram below. We will present the results for both left- and right-handed slepton mixing. But, for simplicity, we will only discuss the case of right-handed slepton mixing explicitly. The amplitudes corresponding to left-handed slepton mixing can be obtained from the right-handed ones by replacing the appropriate hypercharges and slepton masses. Note that for the Z penguin, there is also an additional minus sign after the replacement of hypercharges and slepton masses.

1. Charge radius

The charge radius amplitude $A_\gamma^{L,R}$ comes from the γ penguin, without a chirality flip of the leptons. The dominant term is the one involving the $\tilde{B}$-like neutralino in the loop, with $\tilde{B}$ coupling at each vertex connecting a lepton. The other terms are suppressed either by the muon Yukawa or by two powers of the small bino content in the $\tilde{H}_d^0$-like neutralino. The contributions to the effective vertex of the charge radius is shown in Fig. 5. Summing over these contributions gives[1]

$$A_\gamma^R = \frac{g'^2 (Y_R^l)^2}{576\pi^2} \frac{\sin 2\theta_{\tilde{l}}}{m_{\tilde{l}_1}^2} f_\gamma\left(\frac{M_1^2}{m_{\tilde{l}_1}^2}\right) - (m_{\tilde{l}_1} \to m_{\tilde{l}_2}), \tag{3.20}$$

with

$$f_\gamma(x) = \frac{1}{1-x^4}(2 - 9x + 18x^2 - 11x^3 + 6x^3 \ln x). \tag{3.21}$$

2. Magnetic dipole

The magnetic dipole amplitude $A_{\gamma\text{dip}}^{L,R}$ is the one that appears in $\mu \to e\gamma$, which was discussed in detail in the last section. For right-handed slepton mixing, the amplitude of the dipole term is smaller than the charge radius term, $A_\gamma^{L,R}$, due to the destructive interference between amplitudes involving chirality flips at different locations in the diagram. The situation reverses in the case of left-handed slepton mixing, where both terms contributes and the magnitude becomes larger than the charge radius term.

3. Z penguin

The Z-penguin contribution contains diagrams in Fig. 5, with the photon replaced by the Z boson. The contribution

[1]We have checked that, even when $\mu_d = M_1$, the value given by this expression differs to the exact one by $\lesssim 1\%$. So this expression is valid over all ranges of M_1 and μ_d. The discrepancy comes from the small mass splitting of the neutralinos when the gaugino and Higgsino masses are degenerate. We have used the exact expression in our numerical analysis.

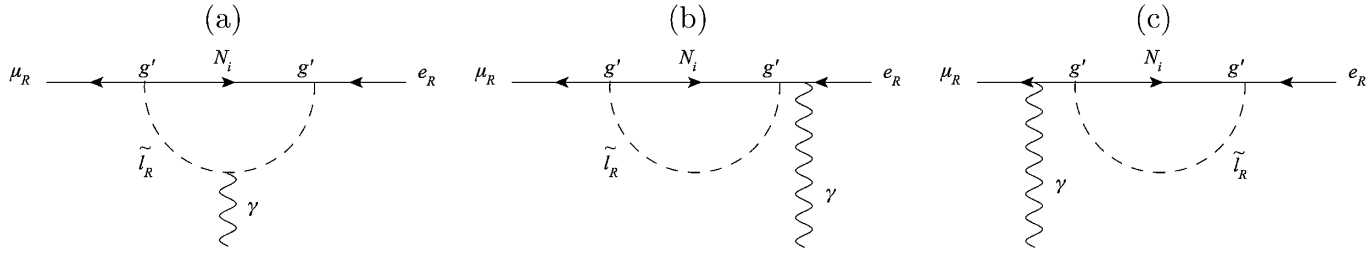

FIG. 5. Contributions to the effective vertex from the charge radius operator. Graph (c) is suppressed by a factor of m_e^2/m_μ^2 compared to (b), and can be ignored in the limit of vanishing electron mass. Also in this limit, graph (b) exactly cancels graph (a) for vanishing photon momentum, satisfying the Ward identity. Only right-handed slepton flavor mixing diagrams are shown, while left-handed slepton flavor mixing diagrams are obtained by swapping $L \leftrightarrow R$.

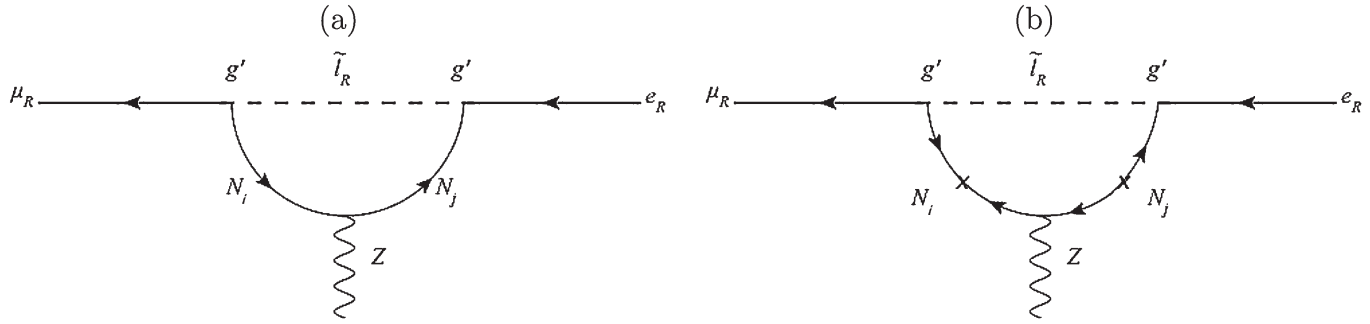

FIG. 6. Contributions to the effective vertex from the Z penguin. Diagram (a) gives the term proportional to f_Z in which the Z boson couples to the R partner of the down-type Higgsino, $\psi_{\tilde{H}_d^0}$, and (b) gives the term proportional to g_Z, with Z coupling to $\tilde{H}_d^0$. Only right-handed slepton flavor mixing diagrams are shown, while left-handed slepton flavor mixing diagrams are obtained by swapping $L \leftrightarrow R$.

coming from this set of diagrams is suppressed by $O(m_\mu^2/M_Z^2)$ compared to the charge radius so is negligible. Then, the dominant term is the one involving a Higgsino-Higgsino-Z vertex, shown in Fig. 6.

We find that the Z penguin is subdominant in a large region of the parameter space. The Z penguin is the only amplitude that is sensitive to $\tan\beta$, and in the limit $M_Z \ll M_N$, it scales as $\cos^2\beta$. The Z-penguin amplitude is

$$A_Z^R = \frac{(Y_R^l)^2 g'^2}{64\pi^2} \frac{\sin 2\theta_{\tilde{l}}}{M_Z^2 \sin^2\theta_w \cos^2\theta_w} \sum_{i,j=1}^{2} \omega_{ij}, \tag{3.22}$$

where

$$\omega_{ij} = O_{Li1} O_{Lj1} \Big[O_{Li2} O_{Lj2} f_Z\Big(\frac{M_{N_i}^2}{m_{\tilde{l}_1}^2}, \frac{M_{N_j}^2}{m_{\tilde{l}_1}^2}\Big) - 2 O_{Ri2} O_{Rj2} g_Z\Big(\frac{M_{N_i}^2}{m_{\tilde{l}_1}^2}, \frac{M_{N_j}^2}{m_{\tilde{l}_1}^2}\Big)\Big] - (m_{\tilde{l}_1} \to m_{\tilde{l}_2}). \tag{3.23}$$

The functions $f_Z(x_i, x_j)$ and $g_Z(x_i, x_j)$ are[2]

$$f_Z(x_i, x_j) = \ln x_i + \frac{1}{x_i - x_j}\Big[\frac{x_i^2 \ln x_i}{1 - x_i} - \frac{x_j^2 \ln x_j}{1 - x_j}\Big], \tag{3.24}$$

$$g_Z(x_i, x_j) = \frac{\sqrt{x_i x_j}}{x_i - x_j}\Big[\frac{x_i \ln x_i}{1 - x_i} - \frac{x_j \ln x_j}{1 - x_j}\Big]. \tag{3.25}$$

Note that the Z-penguin effective vertex does not explicitly depend on $1/M_{\rm SUSY}^2$ as in the case of all other amplitudes. This corresponds to an operator of dimension 4. This is perfectly fine, because the weak symmetry is broken, so the weak current is not conserved. However, it is required that in the limit of unbroken electroweak symmetry, this effective vertex vanishes. This is easy to check in the limit $M_Z \to 0$. In this limit, the neutralinos we consider do not mix [c.f., Eq. (A2)]. But the amplitude for the Z penguin contains at least two powers of the neutralino mixing matrix elements, regardless of whether it is bino-like or Higgsino-like. Therefore, this operator vanishes in the limit $M_Z \to 0$, when the electroweak symmetry is unbroken.

For left-handed sleptons, the Z amplitude can be obtained by replacing the appropriate hypercharges and slepton masses, as well as an additional factor of (-1). This sign change arises from the NNZ coupling, in contrast to $N^c N^c Z$ in the case of right-handed sleptons.

[2]Note that the function f_Z appears to contain a log term that is asymmetric in the two neutralino lines in the loop, not as one would expect. But remember that this log term is subtracted by one containing the heavier slepton mass, and the final result is symmetric in the neutralinos and antisymmetric in the sleptons, as expected.

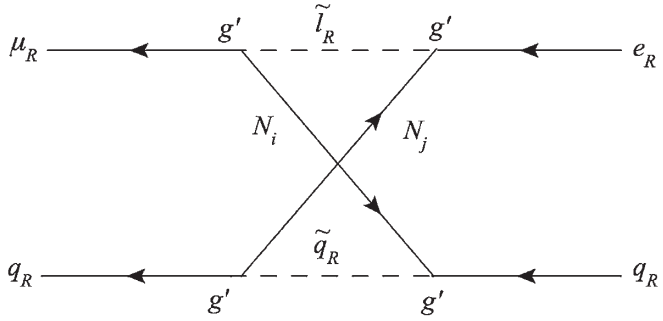

FIG. 7. The box Feynman diagram for $\mu \to e$ conversion. Because of the conservation of R charges, the chirality of the squarks must be the ones shown in the diagrams. Only right-handed slepton flavor mixing diagrams are shown, while left-handed slepton flavor mixing diagrams are obtained by swapping $L \leftrightarrow R$ everywhere.

4. Box diagram

For the box diagram, the dominant term is the one containing bino couplings at all four vertices,

$$A_{\rm box}^{qR} = \frac{(Y_R^l)^2 g'^4 \sin 2\theta_{\tilde{l}}}{64\pi^2 e^2 m_{\tilde{l}_1}^2}\left[(Y_R^q)^2 j_4\left(\frac{M_1^2}{m_{\tilde{l}_1}^2}, \frac{M_1^2}{m_{\tilde{l}_1}^2}, \frac{m_{\tilde{q}_R}^2}{m_{\tilde{l}_1}^2}\right)\right] - (m_{\tilde{l}_1} \to m_{\tilde{l}_2}), \tag{3.26}$$

where

$$j_4(x_i, x_j, y) = \frac{x_i^2 \ln x_i}{(1-x_i)(x_i-x_j)(x_i-y)} - \frac{x_j^2 \ln x_j}{(1-x_j)(x_i-x_j)(x_j-y)} + \frac{y^2 \ln y}{(1-y)(x_i-y)(x_j-y)}. \tag{3.27}$$

We can compare the box amplitude with $A_\gamma^{L,R}$ by approximating $V^{(p)} \simeq V^{(n)}$, giving

$$\left|\frac{A_{\rm box}^R}{A_\gamma^R}\right| = \frac{9(g')^2}{e^2}\frac{j_4(x,x,y)}{f_\gamma(x)}[3(Y_R^d)^2 + 3(Y_R^u)^2] \simeq 19\frac{j_4(x,x,y)}{f_\gamma(x)}, \tag{3.28}$$

where $x = M_1^2/m_{\tilde{l}_1}^2$ and $y = m_{\tilde{q}}^2/m_{\tilde{l}_1}^2$. The right-hand side is plotted in Fig. 8. We can see that the box can give a large contribution the total amplitude when the squarks are not far heavier than the sleptons.

5. Numerical Results

We took $\tan\beta = 3$ for our analysis. The amplitudes contributing to $\mu \to e$ conversion in gold are shown in Fig. 9 for right-handed slepton mixing, and in Fig. 10 for left-handed slepton mixing. The slepton mixing angles are taken to be maximal. For comparison, we also drew the line where the experimental bound on the amplitude would be, as if only one amplitude were contributing to the conversion rate.

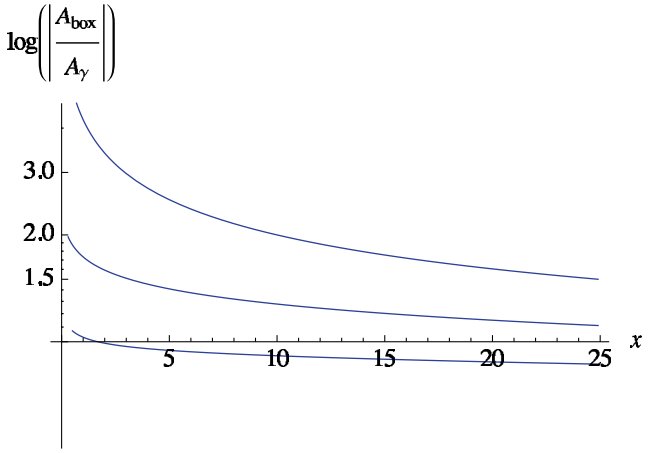

FIG. 8 (color online). A plot of the right-hand side of Eq. (3.28), $19 j_4(x, x, y)/f_\gamma(x)$, where $x = M_1^2/m_{\tilde{l}_1}^2$ and $y = m_{\tilde{q}}^2/m_{\tilde{l}_1}^2$. The contours are $y = 1$, 10, 25 from top to bottom. The box amplitude is larger than the electromagnetic term when the contour is above the x axis.

For right-handed sleptons, either the charge radius or the box diagram dominate over other contributions. Each of these amplitudes exceeds the bound alone and they interfere constructively with each other. Therefore, maximal right-handed slepton mixing is excluded throughout the parameter space we explore. The magnetic dipole destructively interferes with the box and the charge radius diagrams, at small slepton masses before the magnetic dipole vanishes. However, this cancellation is insufficient to bring the amplitudes below the bound.

For both right-handed and left-handed slepton mixing, the Z penguin is subdominant. Moreover, for larger values of $\tan\beta$, the Z penguin will be even more suppressed, since it is directly proportional to $\cos^2\beta = 1/(1+\tan^2\beta)$ to lowest order, in the limit $M_Z \ll M_N$. We show the exclusion plots for $\mu \to e$ conversion in Figs. 11 and 12.

In the left-handed slepton mixing case, the box diagram is suppressed by the left-handed quark hypercharge, and is much smaller. Also, the two largest amplitudes, the charge radius and the magnetic dipole, destructively interfere with each other, resulting in the funnel region shown in Fig. 12.

C. $\mu \to 3e$

Finally, we investigate the decay $\mu^- \to e^- e^+ e^-$. The diagrams that contribute to this decay are similar to the process $\mu \to e$ in a nucleus. While the amplitudes for this decay are not enhanced by nuclear factors as in the case of $\mu \to e$ conversion, there is a log enhancement proportional to $\log m_\mu/m_e$, arising from an infrared divergence cutoff by the electron mass.

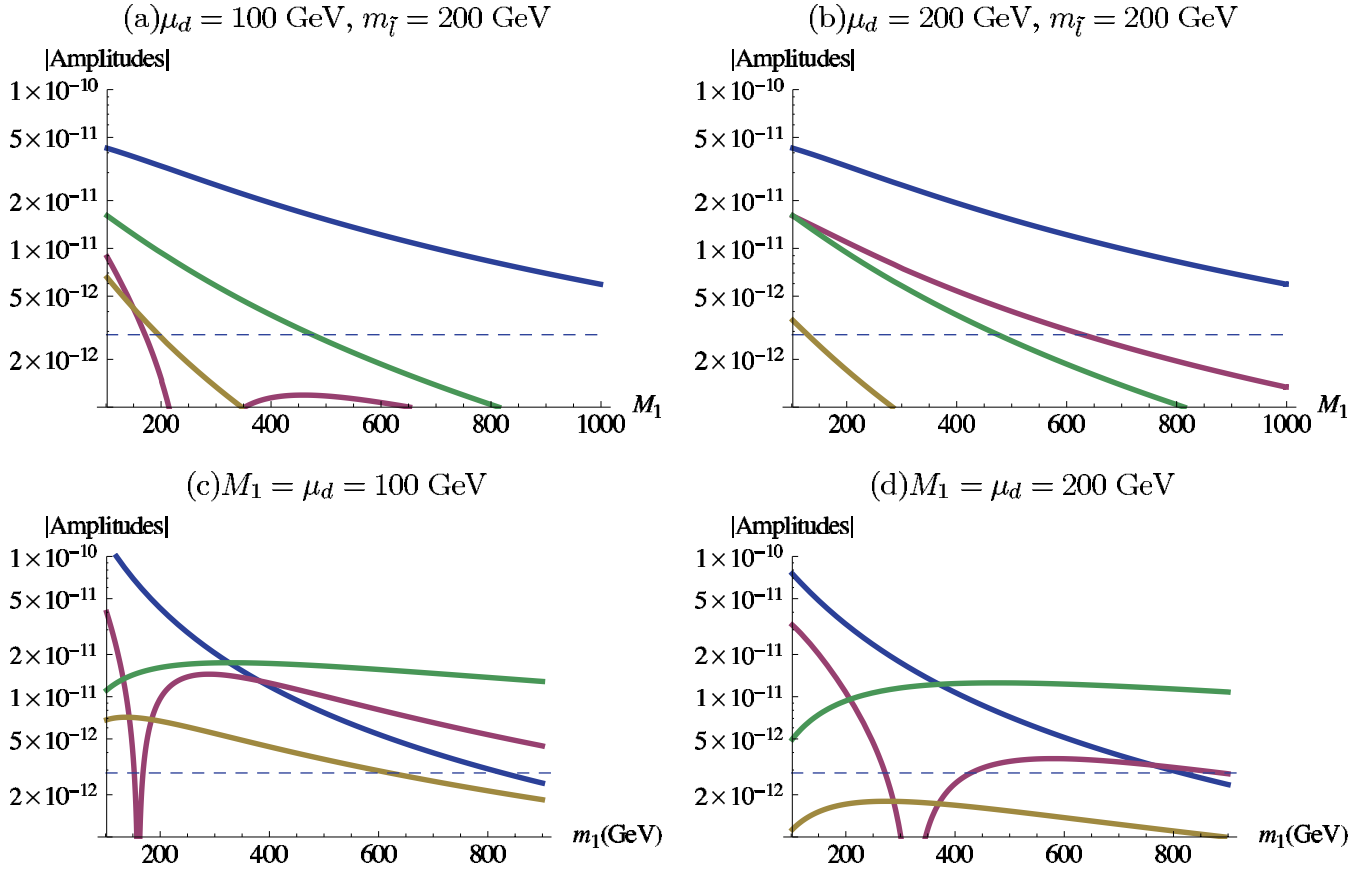

FIG. 9 (color online). The magnitudes of various amplitudes at maximal mixing of right-handed sleptons with degenerate squark masses of 1 TeV (i.e., the terms in Eq. (3.15) before taking the square). The contours are $\mathcal{A}_\gamma^R$ (blue), $\mathcal{A}_{\text{box}}^R$ (green), $|\mathcal{A}_{\gamma\text{dip}}^R|$ (red), and $-\mathcal{A}_Z^R$ (brown). The dashed line corresponds to the bound on $\mu \to e$ conversion as if only one amplitude were contributing. One can see that there are regimes where only the box and the charge radius amplitudes contribute significantly [subfigures (a) and (b), especially in the high M_1 regions in these figures], and where all four amplitudes contribute significantly [subfigure (c)]. In subfigure (d), the magnetic dipole amplitude reaches zero near $m_{\tilde{l}_1} \sim 330$ GeV. This coincides with the "funnel" region in the parameter space plot for $\mu \to e\gamma$, Fig. 2(b). All of the amplitudes, except for the Z penguin, constructively interfere, driving the conversion rate above the experimental bound.

All of the diagrams in $\mu \to 3e$ can be obtained from the $\mu \to e$ conversion diagrams by replacing the quark line by an electron line with outgoing e^+ and e^-. All diagrams except the box are the same and will not be discussed here. For the box, conservation of R charges enforces both sleptons in the loop be of the same "chirality." The box amplitude for $\mu \to 3e$ for right-handed sleptons is

$$B_{\text{box}}^R = \frac{(g' Y_l^R)^4}{16\pi^2 e^2} \sin 2\theta_{\tilde{l}} \sum_{i,k=1}^{2} \frac{(-1)^{i+1}}{m_{\tilde{l}_i}^2} U_k j_4\left(\frac{M_1^2}{m_{\tilde{l}_i}^2}, \frac{M_1^2}{m_{\tilde{l}_i}^2}, \frac{m_{\tilde{l}_k}^2}{m_{\tilde{l}_i}^2}\right), \tag{3.29}$$

where $U_1 = \cos^2\theta_{\tilde{l}}$ and $U_2 = \sin^2\theta_{\tilde{l}}$. The factor $(-1)^{i+1}$ comes from the super-GIM mechanism.

The rate for the decay $\mu \to 3e$ is

$$\begin{aligned}\Gamma_{\mu\to 3e} = \frac{\alpha^2 m_\mu^5}{32\pi}\Big[&(A_\gamma^R)^2 - 4A_\gamma^R A_{\gamma\text{dip}}^L + (A_{\gamma\text{dip}}^L)^2\Big(\frac{16}{3}\log\frac{m_\mu}{m_e} \\ &- \frac{22}{3}\Big) + \frac{1}{6}(B_{\text{box}}^R)^2 + \frac{2}{3}A_\gamma^R B_{\text{box}}^R - \frac{4}{3}A_{\gamma\text{dip}}^L B_{\text{box}}^R \\ &+ \frac{2}{3}F_{RR}^2 + \frac{1}{3}F_{RL}^2 + \frac{2}{3}B_{\text{box}}^R F_{RR} + \frac{4}{3}A_\gamma^R F_{RR} \\ &+ \frac{2}{3}A_\gamma^R F_{RL} - \frac{8}{3}A_{\gamma\text{dip}}^L F_{RR} - \frac{4}{3}A_{\gamma\text{dip}}^L F_{RL}\Big],\end{aligned} \tag{3.30}$$

where $F_{R\alpha} = A_Z^R Z_\alpha^l$, with $\alpha = L, R$. The quantity Z_α is part of the electron-Z coupling; $Z_L = -1/2 + \sin^2\theta_w$, and $Z_R = \sin^2\theta_w$. The branching ratio of this process is obtained by dividing the rate by the muon decay rate. Note that the term proportional to $(A_{\gamma\text{dip}}^L)^2$ is enhanced by the log

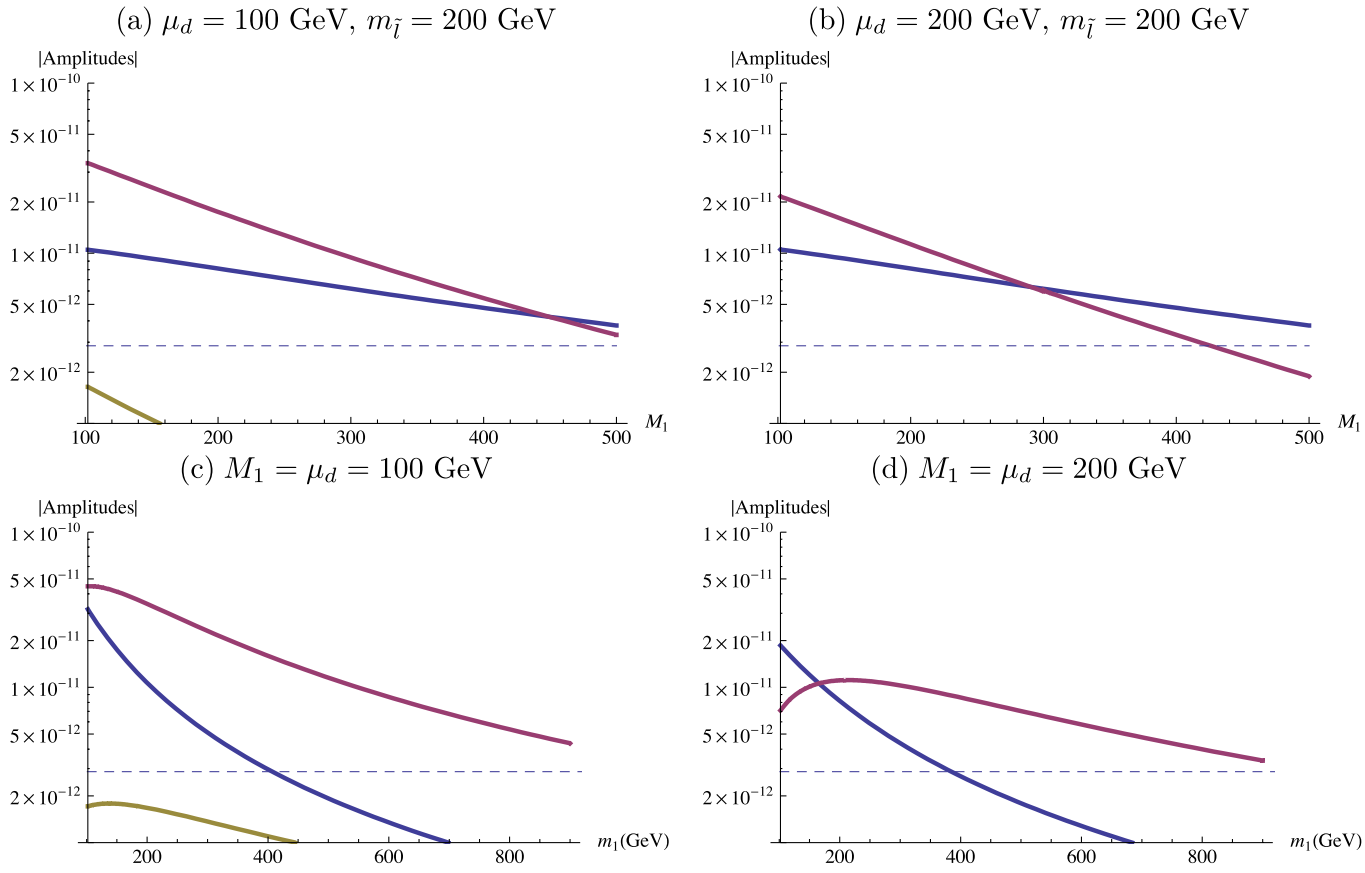

FIG. 10 (color online). Same as Fig. 9 but with left-handed slepton mixing instead. The contours are $\mathcal{A}_\gamma^L$ (blue), $-\mathcal{A}_{\rm box}^L$ (green), $-\mathcal{A}_{\gamma{\rm dip}}^L$ (red), and $\mathcal{A}_Z^L$ (brown). The magnetic dipole and the charge radius amplitudes interfere destructively with each other, opening up a large region in the parameter space that satisfies $\mu \to e$ conversion. This forms the funnel regions in Fig. 12.

term, which is divergent in the limit of massless electrons. Our result for this divergent term agrees with [35].

In Figs. 13 and 14, we show the bounds on the MRSSM parameter space arising from satisfying the existing experimental bound ${\rm BR}(\mu \to 3e) < 1.0 \times 10^{-12}$ from SINDRUM [4]. The bounds on the MRSSM parameter space from $\mu \to 3e$ are weaker than the combined bounds from $\mu \to e\gamma$ and $\mu \to e$ conversion.

IV. IMPLICATIONS FOR FLAVOR VIOLATION SIGNALS AT LHC

One of the most interesting implications of the MRSSM is that flavor mixing could be at or near maximal throughout virtually the entire slepton and squark sector [12] (save only perhaps for $\tilde{d}$-$\tilde{s}$ mixing [36]). For sleptons, this opens up the possibility of observing large μ-e mixing at colliders. Slepton mixing at colliders has been extensively studied [32,37–55], though analyses have generally been relegated to MSSM scenarios where the splitting between the e, μ eigenstates is very small, so as to satisfy the stringent LFV constraints. One of the most sensitive techniques to search for μ-e mixing is through the decay of a heavier neutralino to a lighter one through an on-shell slepton. This decay can arise at a large rate at the LHC starting with squark and/or gluino production, where the squark decays to the heavier neutralino and so on, such as

$$\tilde{q} \to q N_i; \qquad N_i \to e^\pm/\mu^\pm \tilde{l}^\mp; \qquad \tilde{l}^\mp \to \mu^\mp/e^\mp N_j. \tag{4.1}$$

The distinctive kinematic features in this cascade of 2-body decays can be utilized to extract the mass of the slepton through a kinematic edge (e.g., [56–61]).

In light of the bounds on the MRSSM parameter space that we have found from LFV processes, it is interesting to consider whether large mixing could still be seen at the LHC. A detailed collider study is beyond the scope of this paper; nevertheless, we can use our results to uncover characteristic regions of parameter space where $\sin 2\theta_l \sim 1$ simultaneous with several-hundred GeV sparticles, and thus, where large $\mu \leftrightarrow e$ mixing remains within reach of the LHC.

Closely examining Figs. 3(d), 12(d), and 14(d), we discover one (small) region in the MRSSM parameter space where the left-handed slepton mixing angle can be maximal, $\sin 2\theta_l = 1$. For this region, and given first and second

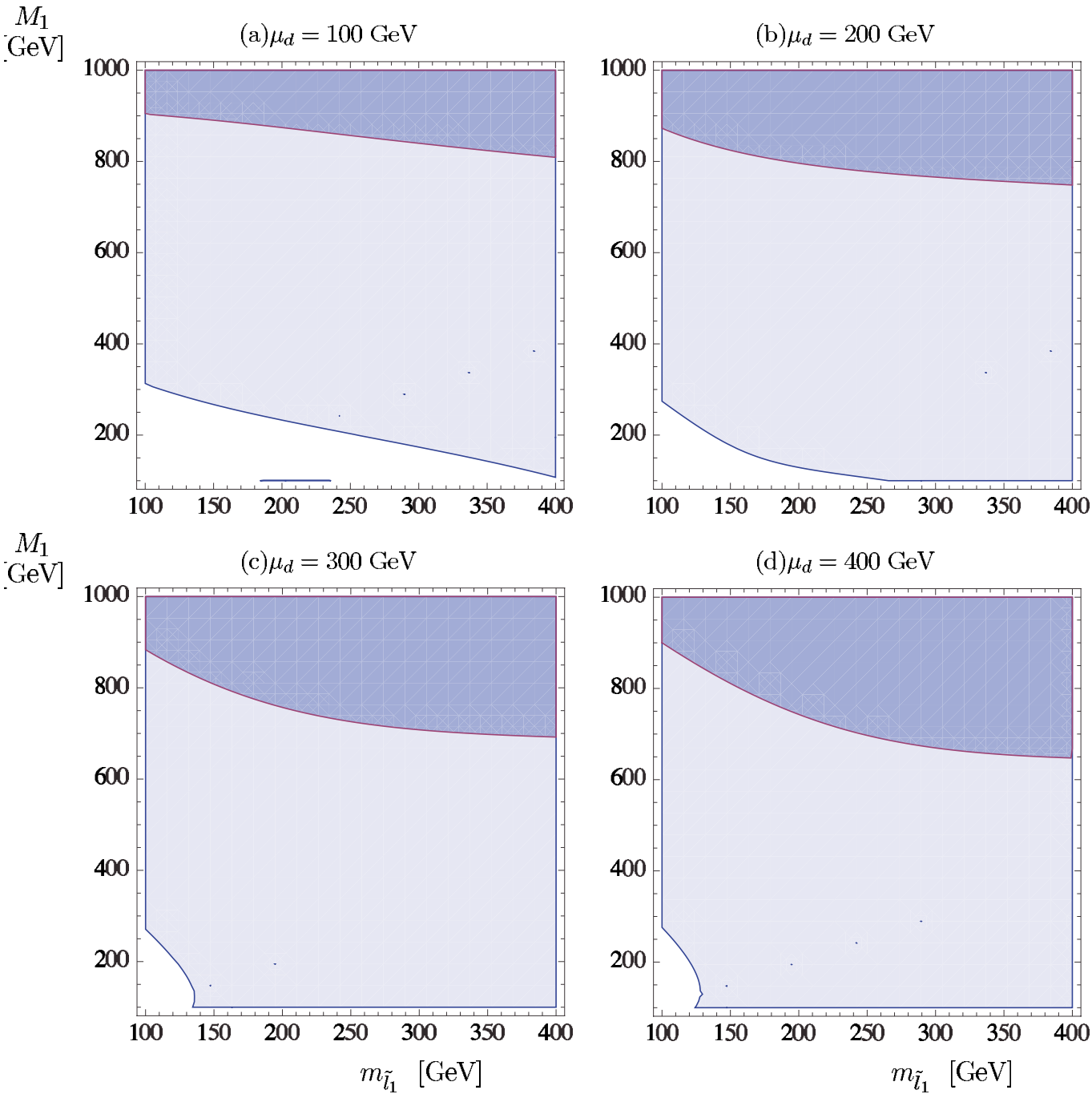

FIG. 11 (color online). Allowable regions for $\mu \rightarrow e$ conversion in a gold nucleus with right-handed slepton mixing. From light to dark, the shaded areas denote mixing with $\sin 2\theta_{\tilde{l}} = 0.1, 0.5$, respectively. The squark masses are set to be degenerate at 1 TeV. Note that this completely rules out maximal mixing for right-handed sleptons in the sub-TeV range.

generation squark masses to be 1 TeV (consistent with what was assumed for the $\mu \rightarrow e$ conversion numerical results), we compute the leading order production cross sections and decay rates. We take the wino mass and the right-handed slepton masses to be 2 TeV for simplicity. The other gaugino masses in this region are $M_1 = 500$ GeV, $\mu_d = 400$ GeV, $\mu_u = 100$ GeV. The mass spectrum is shown in Table I.

Using MADGRAPH [62], we calculated the leading order squark and gluino production cross sections at LHC with $\sqrt{s} = 14$ TeV center of mass energy for several values of the Dirac gluino mass for those production modes allowed by R symmetry in Table II. One important observation made in Ref. [32] is that, for gluinos less than about 2 TeV, associated gluino-squark production gives the largest production rate of squarks.

The decay rates of the squarks, neutralinos, and charginos, computed using BRIDGE [63], can also be computed as a function of the mixing angle θ_l, shown in Table III. For the particular point we considered, the first two generations of squarks decay overwhelmingly into the bino-like neutralino, N_3. The subsequent cascade decays into opposite flavor leptons have the rates $\mathrm{BR}(N_3 \to e\mu N_1) = 0.14 \sin^2 2\theta_l$, $\mathrm{BR}(N_3 \to (ee/\mu\mu) N_1) = 0.27(\sin^4\theta_l + \sin^4\theta_l)$. If the gluino mass is 1 TeV, for example, then the $\tilde{g}\,\tilde{q}$ production leads to a total cross section of about 1 pb. With maximal slepton mixing, the cross section for opposite sign $e\mu$ events is expected to be of order 100 fb. Extracting this signal from background, particularly given the potentially problematic technique of flavor-subtraction, remains challenging. (See Ref. [32] for a discussion of signal plus background analysis of a nonminimal R-symmetric model.)

Just as in the MSSM, one can search for the kinematic endpoint in the invariant mass distribution of the leptons.

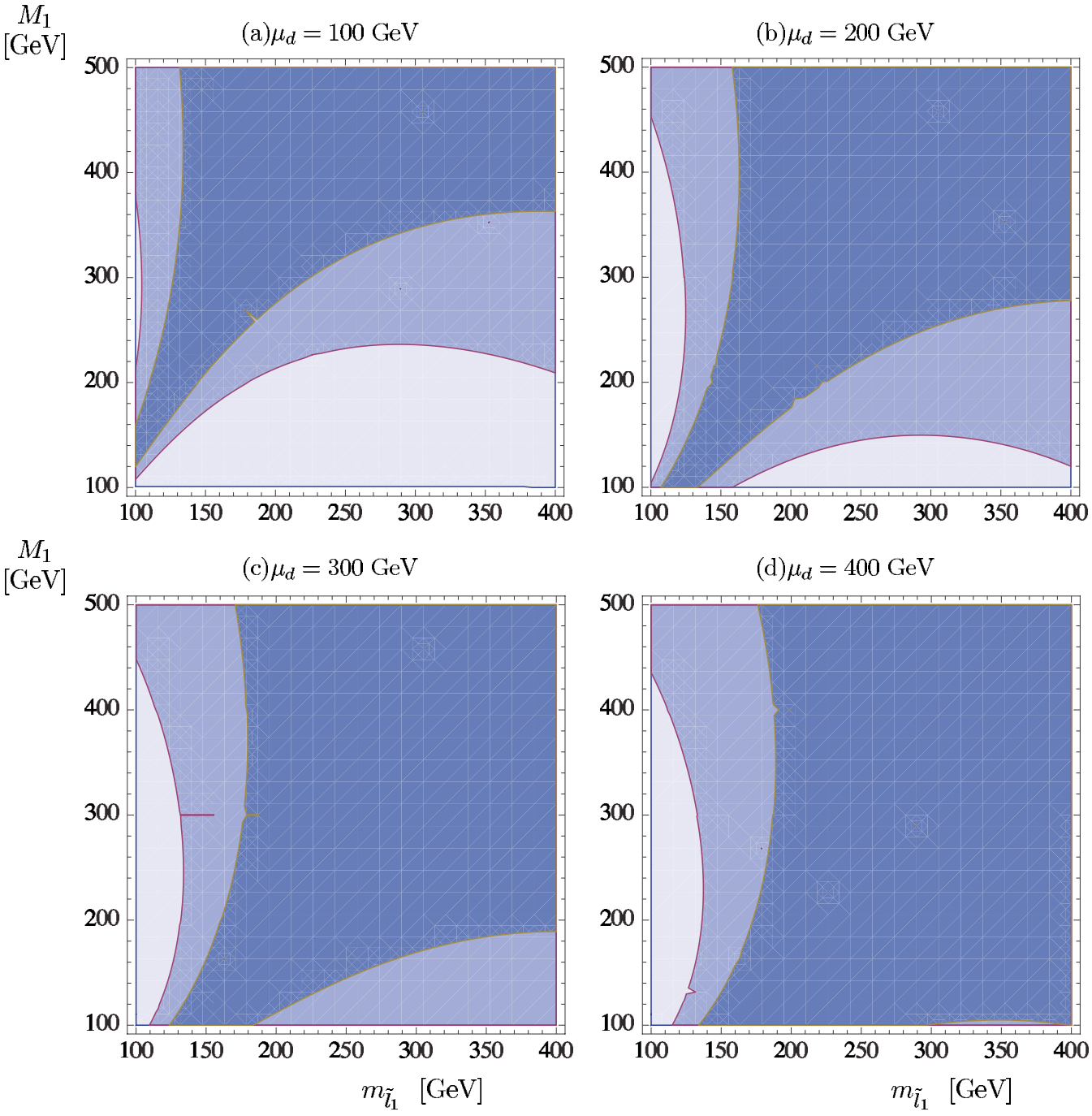

FIG. 12 (color online). Same for Fig. 11 but with left-handed slepton mixing instead.

In the MRSSM, however, the two slepton mass eigenstates are not near one another, and so two distinct and well-separated kinematic edges could in principle be extracted. This would be a striking signal of slepton flavor violation in the MRSSM. Note also that the electric charges of the leptons in this decay are fixed by the conversation of R charges. For example, the antineutralino N_3^c can decay into $l^+\tilde{l}_L^-$, the decay into the same final state for N_3 is forbidden.

V. DISCUSSION

We have calculated the constraints on $\mu \leftrightarrow e$ mixing in the MRSSM from the flavor-violating processes $\mu \rightarrow e\gamma$, $\mu \rightarrow e$ conversion, and $\mu \rightarrow 3e$. Given the simplifications stated in Sec. II, we explored LFV in the MRSSM as a function of the parameters M_1, μ_d, $m_{\tilde{l}}$, and $\sin 2\theta_{\tilde{l}}$ within the sub-TeV range. Given the heavier slepton mass set to be $m_{\tilde{l}_2} = 1.5 m_{\tilde{l}_2}$, we found that the bound from $\mu \rightarrow 3e$ is

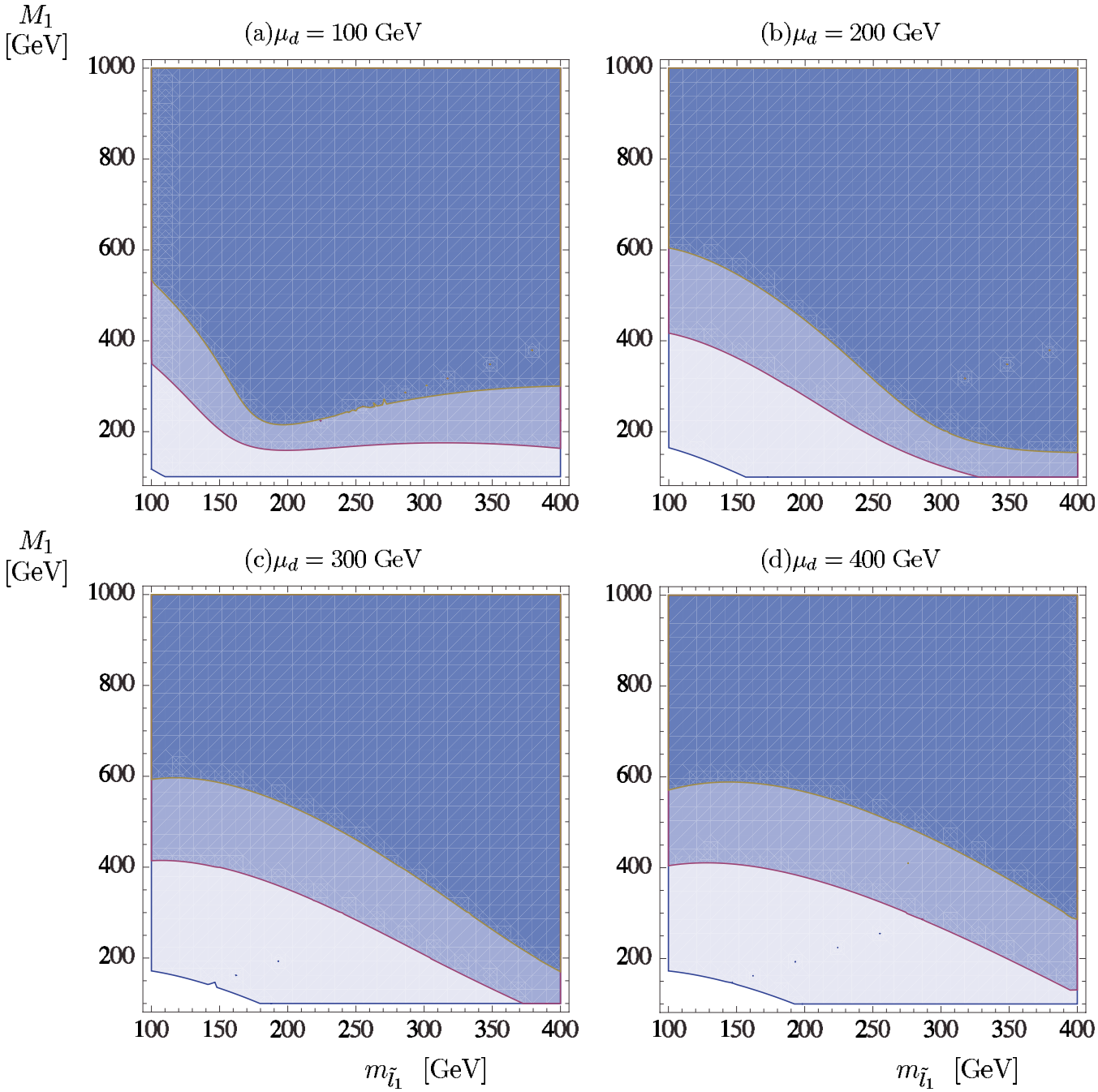

FIG. 13 (color online). Regions of the parameter space that satisfy the $\mu \rightarrow 3e$ bound at different mixing angles of right-handed sleptons. The values of $\sin 2\theta_{\tilde{l}}$ are, from light to dark, 0.1, 0.5, 1.

always less severe than the bounds derived from either $\mu \to e\gamma$ or $\mu \to e$ conversion. We show the overlapping regions allowed by all constraints in Figs. 15 and 16.

For right-handed slepton mixing, $\mu \to e$ conversion in gold nuclei provides the most severe constraint—it completely rules out maximal mixing (compare Fig. 15 with Fig. 2). The situation is qualitatively different for left-handed mixing—the most severe bound in this case comes from $\mu \to e\gamma$, as dominant amplitudes (charge radius and magnetic dipole) of $\mu \to e$ conversion interfere destructively and opens up a large region in parameter space that satisfies the experimental bounds. From Fig. 3 for $\mu \to e\gamma$, one sees that maximal mixing is allowed in regions where the bino mass is $\sim$500 GeV at $\mu_d = 200$ GeV, with a moderate splitting between sleptons. The results suggest that the most likely observation of large slepton flavor violation signals at the LHC will occur in the left-handed sector.

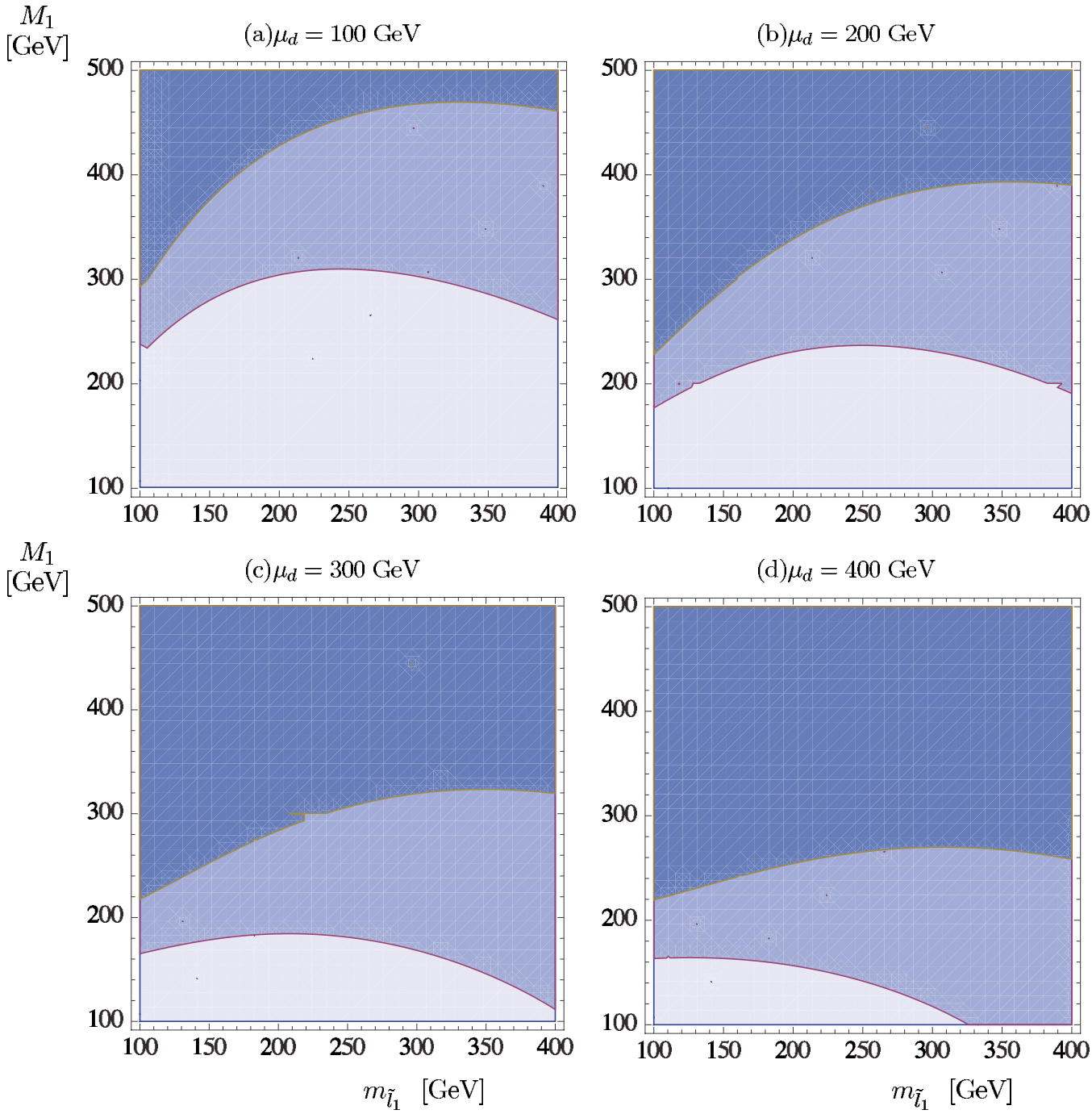

FIG. 14 (color online). Same as Fig. 13 but with left-handed slepton mixing.

Finally, is interesting to consider how the bounds on slepton flavor mixing angles will change as the constraints on LFV are strengthened. This is most easily understood by recognizing that all of our bounds are proportional to $\sin^2 2\theta_{\tilde{l}}$. In other words, the boundary of the allowed regions are contours of constant $\mathrm{BR}_{\mathrm{bound}}/\sin^2 2\theta_{\tilde{l}}$, where $\mathrm{BR}_{\mathrm{bound}}$ is the bound on the branching ratio of a process. In plotting the allowed regions of parameter space in the previous sections of the paper, we used of course the current experimental bound. Suppose that in some future experiment the bounds are improved, say by a factor of 100. Then, the boundary of the region that satisfy this new bound for $\sin^2 2\theta_{\tilde{l}} = 0.1$ is the same as the boundary for the current bound with $\sin^2 2\theta_{\tilde{l}} = 1$.

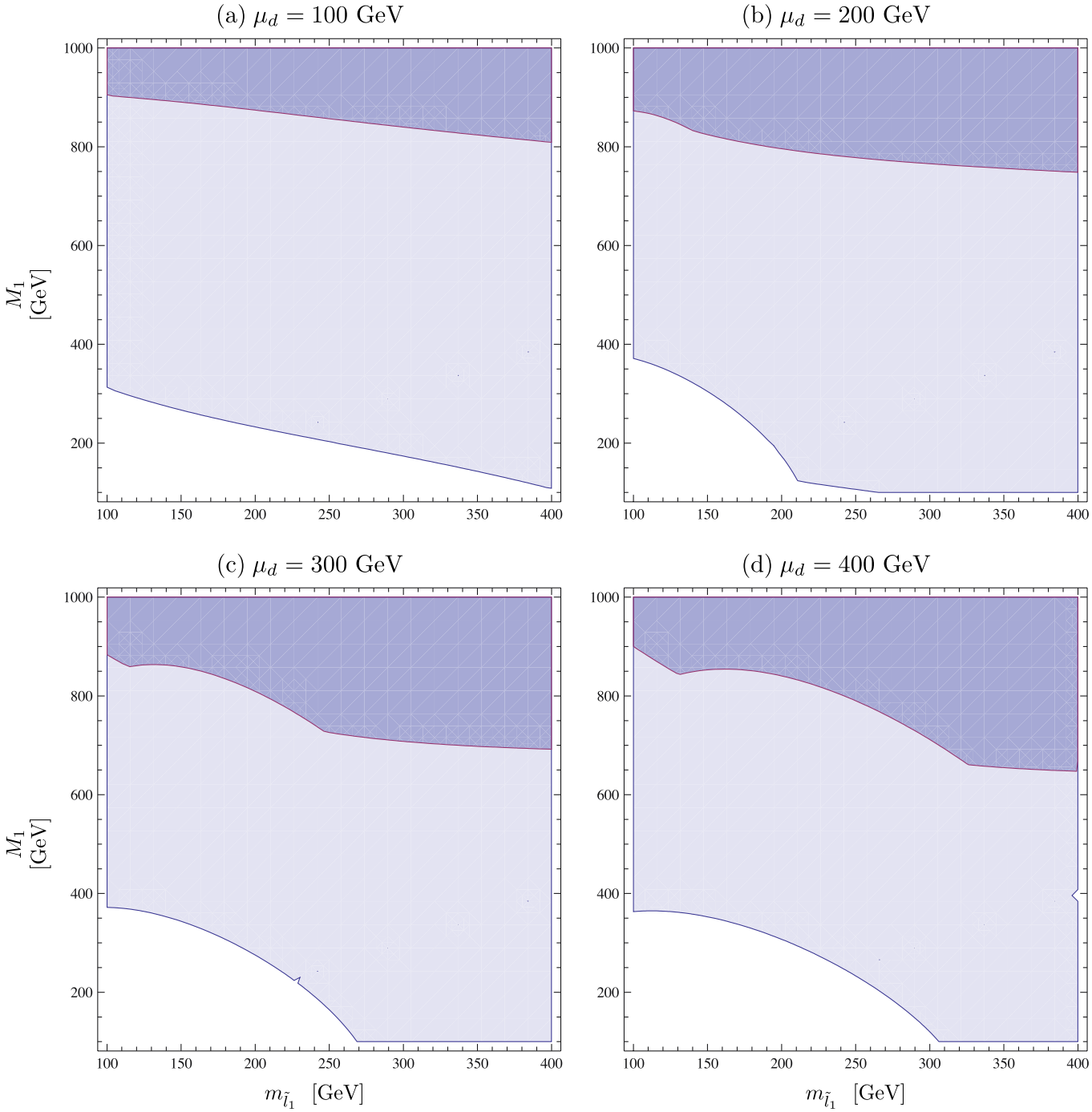

FIG. 15 (color online). Regions allowed in the parameter space by combining the three constraints for right-handed sleptons. The constraint from $\mu \to 3e$ is always less severe than the other two processes in the parameter space shown.

ACKNOWLEDGMENTS

We thank A. Martin and T. Roy for discussions as well as invaluable assistance in running MADGRAPH with the MRSSM model. We also thank D. Tucker-Smith for clarifications of some of the results in Ref. [32]. This work was supported in part by the Department of Energy under Contract No. DE-FG02-96ER40969.

APPENDIX: GAUGINO AND SLEPTON STRUCTURE

To discuss the neutralino masses and interactions more quantitatively, we define the ψ_B and $\psi_{\tilde{H}_d}$ to the be fermion R partners of $\tilde{B}$ and $\tilde{H}_d^0$, respectively. Then, we form the Dirac bino and Higgsino spinors and their charge conjugates,

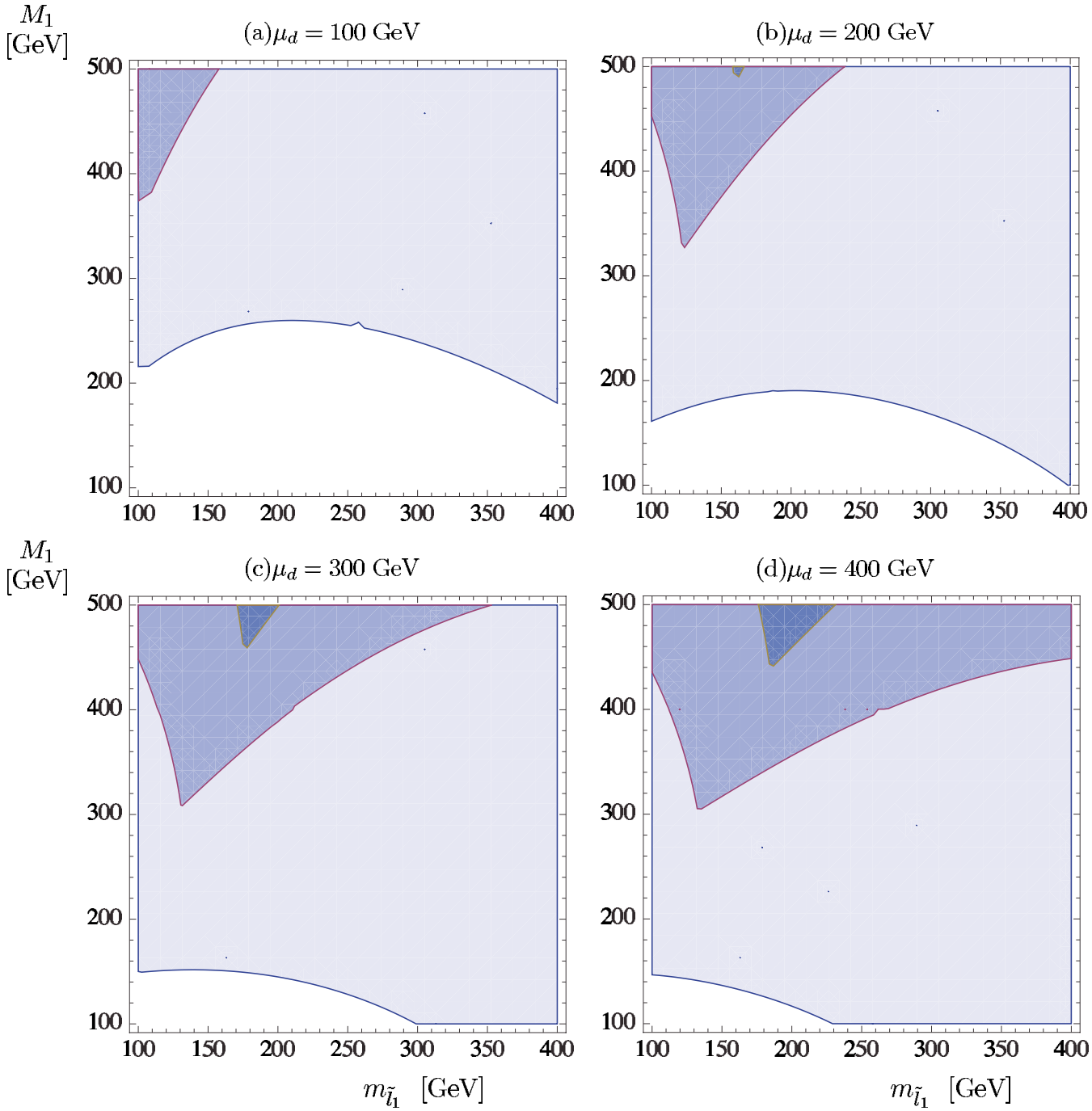

FIG. 16 (color online). Same as Fig. 15 but for left-handed sleptons. Similar to the right-handed case, the constraint from $\mu \to 3e$ is also less severe than the other two processes in the parameter space shown.

TABLE I. Mass spectrum.

Particle	$\tilde{q}_{L,R}$	$\tilde{g}$	$N_3 \simeq \tilde{B}$	$C_2 \simeq \tilde{H}_d$	$N_2 \simeq \tilde{H}_d$	$\tilde{l}_{L2}$	$\tilde{l}_{L1}$	$C_1 \simeq \tilde{H}_u$	$N_1 \simeq \tilde{H}_u$
Mass (GeV)	1000	1000	502	400	400	270	180	100	100

TABLE II. Leading order production cross sections for squarks and gluinos at the LHC with $\sqrt{s} = 14$ TeV in the MRSSM.

$M_{\tilde{g}}$ (TeV)	$\tilde{g}$-$\tilde{q}_{L,R}$	$\tilde{q}_R$-$\tilde{q}_L$	$\tilde{q}$-$\tilde{q}^*$	$\tilde{g}$-$\tilde{g}$	σ (fb)
1	810	120	50	330	1300
2	36	31	27	1.0	95
3	2.6	11	22	0.007	35

$$N_{\tilde{B}} = \begin{pmatrix} \psi_B \\ \tilde{B}^\dagger \end{pmatrix}, \qquad N_{\tilde{H}_d} = \begin{pmatrix} \tilde{H}_d^0 \\ \psi^\dagger_{\tilde{H}_d} \end{pmatrix},$$
$$N^c_{\tilde{B}} = \begin{pmatrix} \tilde{B} \\ \psi_B^\dagger \end{pmatrix}, \qquad N^c_{\tilde{H}_d} = \begin{pmatrix} \psi_{\tilde{H}_d} \\ \tilde{H}_d^{0\dagger} \end{pmatrix}. \tag{A1}$$

We can also see that the Dirac spinor N has an R charge of -1; whereas, N^c has an R charge of $+1$. The gaugino mass matrix, M_N, is shown in the mass term below

$$(\bar{N}_B, \bar{N}_{\tilde{H}_d}) \begin{pmatrix} M_1 & -\cos\beta \sin\theta_W M_Z \\ 0 & \mu_d \end{pmatrix} \begin{pmatrix} P_L N_B \\ P_L N_{\tilde{H}_d} \end{pmatrix} + \text{H.c.} \tag{A2}$$

The mass matrix is diagonalized by a bi-orthogonal transformation; the diagonalized neutralino mass matrix, $M_N^D = O_L^T M_N O_R$, obeys $(M_N^D)^2 = O_L M_N (M_N)^T \times (O_L)^T = O_R (M_N)^T M_N (O_R)^T$, where $O_{(L,R)}$ are the orthogonal matrices that diagonalize the mass matrix. In this definition, the $\tilde{B}$ and $\tilde{H}_d^0$ content of the ith neutralino N_i are, O_{Li1} and O_{Ri2}, respectively.

We consider mixing between selectrons and smuons only, parametrized as follows:

$$\begin{pmatrix} \tilde{l}_1 \\ \tilde{l}_2 \end{pmatrix}_{L,R} = \begin{pmatrix} \cos\theta_{\tilde{l}} & \sin\theta_{\tilde{l}} \\ -\sin\theta_{\tilde{l}} & \cos\theta_{\tilde{l}} \end{pmatrix}_{L,R} \begin{pmatrix} \tilde{e} \\ \tilde{\mu} \end{pmatrix}_{L,R}, \tag{A3}$$

where $\tilde{l}_i$ represents the sleptons in the mass eigenstate basis.

Then, slepton flavor violation comes from the interaction terms between a sfermion, $\tilde{f}_i$, a neutralino, N_i, and a fermion f_i:

$$-\tilde{f}^*_{L\alpha} \bar{N}_i (U^\dagger_{L\alpha\beta} [O_{Li1} G_L f_{L\beta} + O_{Ri2} y_f f_{R\beta}]) - \tilde{f}^*_{R\alpha} \bar{N}^c_i (U^\dagger_{R\alpha\beta} [O_{Li1} G_R f_{R\beta} + O_{Ri2} y_f f_{L\beta}]) + \text{H.c.}, \tag{A4}$$

where $U_{L,R}$ are the slepton mixing matrices in Eq. (A3). The coupling constants are

TABLE III. Decay branching ratios of the particles involved in the cascade decay $N_3 \to l^- \tilde{l}_L^+ \to l^- l'^+ N_1$ given the MRSSM parameters given in Table I.

Decaying particle	Decay modes	Branching ratios
$\tilde{q}$	qN_3	0.99
N_3	ZN_2	8×10^{-4}
	ZN_1	0.12
	$C_2^- W^+$	0.02
	$C_1^+ W^-$	0.22
	$\nu\tilde{\nu}_1$	0.19
	$\nu\tilde{\nu}_2$	0.13
	$e^- \tilde{l}^+_{L1}$	$0.19\cos^2\theta_l$
	$\mu^- \tilde{l}^+_{L1}$	$0.19\sin^2\theta_l$
	$e^- \tilde{l}^+_{L2}$	$0.13\sin^2\theta_l$
	$\mu^- \tilde{l}^+_{L2}$	$0.13\cos^2\theta_l$
$\tilde{l}^+_{L1}$	$C_1^+ \bar{\nu}$	0.11
	$N_1 e^+$	$0.88\cos^2\theta_l$
	$N_1 \mu^+$	$0.88\sin^2\theta_l$
$\tilde{l}^+_{L2}$	$C_1^+ \bar{\nu}$	0.16
	$N_1 e^+$	$0.84\sin^2\theta_l$
	$N_1 \mu^+$	$0.84\cos^2\theta_l$

$$G_{L,R} = \sqrt{2} g' Y_{f_{(L,R)}}, \quad \text{and} \tag{A5}$$

$$y_f = \frac{g' m_f}{\sqrt{2} M_Z \sin\theta_w \cos\beta}. \tag{A6}$$

The subscript i on the (s)fermion denotes its generation, subscripts L and R denote the chirality, with α and β being the flavor indices. The hypercharge of a fermion f is denoted by Y_f. From the above interaction terms we see that $\tilde{f}_R$ and $\tilde{f}_L$ have different R charges: -1 and $+1$, respectively.

The Z boson only couples to Higgsinos. The ZNN interaction term is

$$\frac{g}{2\cos\theta_w} Z_\mu [\bar{N}_i \gamma^\mu (O_{Ri2} O_{Rj2} P_L + O_{Li2} O_{Lj2} P_R) N_j]. \tag{A7}$$

One can also write the ZNN coupling in terms of N^c,

$$-\frac{g}{2\cos\theta_w} Z_\mu [\bar{N^c}_i \gamma^\mu (O_{Li2} O_{Lj2} P_L + O_{Ri2} O_{Rj2} P_R) N^c_j]. \tag{A8}$$

Examining the neutralino mixing matrix in Eq. (A2), the lightest gaugino receives a negative shift, $-\Delta < 0$, and so the lightest neutralino has mass $M_{N_1} = \mu_d - \Delta < m_{C_1}$, and thus the lightest gaugino is a neutralino.

[1] M. Ahmed *et al.* (MEGA Collaboration), Phys. Rev. D **65**, 112002 (2002).
[2] J. Adam *et al.* (MEG Collaboration), Nucl. Phys. **B834**, 1 (2010).
[3] W. H. Bertl *et al.* (SINDRUM II Collaboration), Eur. Phys. J. C **47**, 337 (2006).
[4] U. Bellgardt *et al.* (SINDRUM Collaboration), Nucl. Phys **B299**, 1 (1988).
[5] R. K. Kutschke, AIP Conf. Proc. **1182**, 718 (2009).
[6] Project X and the Science of the Intensity Frontier, white paper, Fermilab, 2010, http://www.fnal.gov/pub/projectx/pdfs/ProjectXwhitepaperJan.v2.pdf.
[7] J. Hisano, T. Moroi, K. Tobe, and M. Yamaguchi, Phys. Rev. D **53**, 2442 (1996).
[8] J. Hisano and D. Nomura, Phys. Rev. D **59**, 116005 (1999).
[9] I. Masina and C. A. Savoy, Nucl. Phys. **B661**, 365 (2003).
[10] P. Paradisi, J. High Energy Phys. 10 (2005) 006.
[11] M. Ciuchini, A. Masiero, P. Paradisi, L. Silvestrini, S. K. Vempati, and O. Vives, Nucl. Phys. **B783**, 112 (2007).
[12] G. D. Kribs, E. Poppitz, and N. Weiner, Phys. Rev. D **78**, 055010 (2008).
[13] G. D. Kribs, A. Martin, and T. S. Roy, J. High Energy Phys. 01 (2009) 023.
[14] P. Fayet, Phys. Lett. **78B**, 417 (1978).
[15] J. Polchinski and L. Susskind, Phys. Rev. D **26**, 3661 (1982).
[16] L. J. Hall and L. Randall, Nucl. Phys. **B352**, 289 (1991).
[17] P. J. Fox, A. E. Nelson, and N. Weiner, J. High Energy Phys. 08 (2002) 035.
[18] A. E. Nelson, N. Rius, V. Sanz, and M. Unsal, J. High Energy Phys. 08 (2002) 039.
[19] Z. Chacko, P. J. Fox, and H. Murayama, Nucl. Phys. **B706**, 53 (2005).
[20] L. M. Carpenter, P. J. Fox, and D. E. Kaplan, arXiv:hep-ph/0503093.
[21] I. Antoniadis, K. Benakli, A. Delgado, and M. Quiros, Adv. Theor. Phys. **2**, 645 (2008).
[22] J. Hisano, M. Nagai, T. Naganawa, and M. Senami, Phys. Lett. B **644**, 256 (2007).
[23] K. Hsieh, Phys. Rev. D **77**, 015004 (2008).
[24] S. Y. Choi, M. Drees, A. Freitas, and P. M. Zerwas, Phys. Rev. D **78**, 095007 (2008).
[25] S. D. L. Amigo, A. E. Blechman, P. J. Fox, and E. Poppitz, J. High Energy Phys. 01 (2009) 018.
[26] T. Plehn and T. M. P. Tait, J. Phys. G **36**, 075001 (2009).
[27] R. Harnik and G. D. Kribs, Phys. Rev. D **79**, 095007 (2009).
[28] K. Benakli and M. D. Goodsell, Nucl. Phys. **B816**, 185 (2009).
[29] M. Luo and S. Zheng, J. High Energy Phys. 01 (2009) 004.
[30] G. D. Kribs, A. Martin, and T. S. Roy, J. High Energy Phys. 06 (2009) 042.
[31] A. E. Blechman, Mod. Phys. Lett. A **24**, 633 (2009).
[32] A. Kumar, D. Tucker-Smith, and N. Weiner, arXiv:0910.2475.
[33] R. Kitano, M. Koike, and Y. Okada, Phys. Rev. D **66**, 096002 (2002); **76**, 059902(E) (2007).
[34] V. Cirigliano, R. Kitano, Y. Okada, and P. Tuzon, Phys. Rev. D **80**, 013002 (2009).
[35] A. De Gouvea, G. F. Giudice, A. Strumia, and K. Tobe, Nucl. Phys. **B623**, 395 (2002).
[36] A. E. Blechman and S. P. Ng, J. High Energy Phys. 06 (2008) 043.
[37] S. I. Bityukov and N. V. Krasnikov, Yad. Fiz. **62**, 1288 (1999) [Phys. At. Nucl. **62**, 1213 (1999)].
[38] K. Agashe and M. Graesser, Phys. Rev. D **61**, 075008 (2000).
[39] J. Hisano, R. Kitano, and M. M. Nojiri, Phys. Rev. D **65**, 116002 (2002).
[40] J. Kalinowski, Acta Phys. Pol. B **33**, 2613 (2002).
[41] F. Deppisch, J. Kalinowski, H. Pas, A. Redelbach, and R. Ruckl, arXiv:hep-ph/0401243.
[42] T. Goto, K. Kawagoe, and M. M. Nojiri, Phys. Rev. D **70**, 075016 (2004); **71**, 059902(E) (2005).
[43] K. Hamaguchi and A. Ibarra, J. High Energy Phys. 02 (2005) 028.
[44] Yu. M. Andreev, S. I. Bityukov, N. V. Krasnikov, and A. N. Toropin, Phys. At. Nucl. **70**, 1717 (2007).
[45] Y. Grossman, Y. Nir, J. Thaler, T. Volansky, and J. Zupan, Phys. Rev. D **76**, 096006 (2007).
[46] J. L. Feng, C. G. Lester, Y. Nir, and Y. Shadmi, Phys. Rev. D **77**, 076002 (2008).
[47] Y. Nomura, M. Papucci, and D. Stolarski, Phys. Rev. D **77**, 075006 (2008).
[48] R. Kitano, J. High Energy Phys. 03 (2008) 023.
[49] B. C. Allanach, J. P. Conlon, and C. G. Lester, Phys. Rev. D **77**, 076006 (2008).
[50] M. Hirsch, J. W. F. Valle, W. Porod, J. C. Romao, and A. Villanova del Moral, Phys. Rev. D **78**, 013006 (2008).
[51] S. Kaneko, J. Sato, T. Shimomura, O. Vives, and M. Yamanaka, Phys. Rev. D **78**, 116013 (2008).
[52] J. Hisano, M. M. Nojiri, and W. Sreethawong, J. High Energy Phys. 06 (2009) 044.
[53] J. L. Feng, I. Galon, D. Sanford, Y. Shadmi, and F. Yu, Phys. Rev. D **79**, 116009 (2009).
[54] J. L. Feng *et al.*, arXiv:0910.1618.
[55] A. J. Buras, L. Calibbi, and P. Paradisi, arXiv:0912.1309.
[56] I. Hinchliffe, F. E. Paige, M. D. Shapiro, J. Soderqvist, and W. Yao, Phys. Rev. D **55**, 5520 (1997).
[57] S. Abdullin *et al.* (CMS Collaboration), J. Phys. G **28**, 469 (2002).
[58] H. Bachacou, I. Hinchliffe, and F. E. Paige, Phys. Rev. D **62**, 015009 (2000).
[59] I. Hinchliffe and F. E. Paige, Phys. Rev. D **61**, 095011 (2000).
[60] B. C. Allanach, C. G. Lester, M. A. Parker, and B. R. Webber, J. High Energy Phys. 09 (2000) 004.
[61] G. Aad *et al.* (ATLAS Collaboration), arXiv:0901.0512.
[62] J. Alwall *et al.*, J. High Energy Phys. 09 (2007) 028.
[63] P. Meade and M. Reece, arXiv:hep-ph/0703031.